RMetS
Royal Meteorological Society

Observations of the convective environment in developing and non-developing tropical disturbances

Roger K. Smith[a]* and Michael T. Montgomery[b,c]†

[a]*Meteorological Institute, Ludwig-Maximilians University, Munich, Germany*
[b]*Dept. of Meteorology, Naval Postgraduate School, Monterey, California, USA*
[c]*Hurricane Research Division, NOAA, Miami, Florida, USA*

*Correspondence to: R. K. Smith, Meteorological Institute, Ludwig-Maximilians University, Theresienstrasse 37, 80333 Munich, Germany. E-mail: roger.smith@lmu.de

†The contribution of M. T. Montgomery to this article was prepared as part of his official duties as a US Federal Government employee.

Analyses of thermodynamic data gathered from airborne dropwindsondes released from the upper troposphere during the Pre-Depression Investigation of Cloud Systems in the Tropics (PREDICT) experiment are presented. We focus on two systems that finally became hurricanes *Karl* and *Matthew*, and one system (*Gaston*) that attained tropical storm status, but subsequently weakened and never redeveloped during five days of monitoring. Data for all events show that the largest values of total precipitable water are collocated with the surface trough and with values of convective available potential energy that seem high enough to support convective organization. These values coincide mostly with low values of convective inhibition. Vertical profiles of virtual potential temperature show little variability between soundings on a particular day, but the system means from day to day show a slight warming. In contrast, vertical profiles of pseudo-equivalent potential temperature, θ_e, show much more variability between soundings on a particular day on account of the variability in moisture.

In all systems, there was is a tendency for the lower troposphere to moisten, but in the non-developing system, the troposphere became progressively drier in the height range between approximately 2 and 9 km during the five days of observations. In the developing systems, the troposphere moistened. The most prominent difference between the non-developing system and the two developing systems was the much larger reduction of θ_e between the surface and a height of 3 km, typically 25 K in the non-developing system, compared with only 17 K in the developing systems. Conventional wisdom would suggest that, for this reason, the convective downdraughts would be stronger in the non-developing system and would thereby act to suppress the development. Here we propose an alternative hypothesis in which the drier air weakens the convective updraughts and thereby the convective amplification of absolute vorticity necessary for development.

Key Words: tropical cyclogenesis; hurricane formation; hurricane spin-up; cyclone intensification; PREDICT; GRIP; IFEX

Received 23 June 2011; Revised 8 January 2012; Accepted 26 January 2012; Published online in Wiley Online Library 19 June 2012

Citation: Smith RK, Montgomery MT. 2012. Observations of the convective environment in developing and non-developing tropical disturbances. *Q. J. R. Meteorol. Soc.* **138**: 1721–1739. DOI:10.1002/qj.1910

1. Introduction

Understanding the dynamics of tropical cyclogenesis remains one of the great unsolved problems in tropical meteorology. One reason for the lack of understanding is undoubtedly the fact that genesis occurs over the tropical oceans where conventional observational data such as radar data, radiosonde soundings and surface data are relatively sparse. While there have been a few field experiments directed at documenting cyclogenesis (Bister and Emanuel, 1997; Ritchie and Holland, 1999; Halverson *et al.*, 2007; Elsberry and Harr, 2008; Zipser *et al.*, 2009) and a few serendipitous sets of measurements (Reasor *et al.*, 2005; Houze *et al.*, 2009), many questions remain about the processes involved and their relative importance. A recent review of work over the past few years is given by Montgomery and Smith (2011).

In the late summer of 2010, a trio of field experiments was conducted by the National Aeronautics and Space Administration (NASA), National Oceanic and Atmospheric Administration (NOAA) and National Science Foundation (NSF) to investigate tropical cyclogenesis in the Caribbean and West Atlantic and the subsequent intensification of storms in these regions. While two of the experiments* included intensification in their portfolio of objectives, the Pre-Depression Investigation of Cloud Systems in the Tropics (PREDICT) experiment was designed exclusively to study genesis. Priority was given to developing storms prior to their classification as tropical depressions as defined by forecasters†, even when mature storms were present nearby. The primary measurement platform of PREDICT was the National Center for Atmospheric Research (NCAR) GV research aircraft, equipped with dropsondes and onboard sensors for meteorological variables and ice microphysics. The range and speed of the GV, and the high altitude ($\approx$13–14 km) from which it could release dropsondes, were exploited to sample storm formation from Central America to the mid-Atlantic (roughly 40°W) operating out of St. Croix in the US Virgin Islands. Some measurements were made also by the NASA DC8 research aircraft, which has the capability to release dropsondes from moderately high in the troposphere ($\approx$10–11 km).

The PREDICT field experiment aimed to gather data on developing and non-developing tropical disturbances and to test the recently proposed marsupial model of tropical cyclogenesis in association with tropical easterly waves (Dunkerton *et al.*, 2009). The overarching hypothesis was that tropical depression formation is greatly favoured in the critical-layer region of the synoptic-scale, pre-depression wave or subtropical disturbance. A summary of the scientific basis for the experiment as well as some highlights of the data obtained was described by Montgomery *et al.* (2012). The experiment collected, *inter alia*, unprecedented‡ dropwindsonde data from two high-altitude flying aircraft (the NCAR GV and NASA DC-8). When these aircraft were flying the same system, the flights were staggered in time to provide an optimum temporal coverage. The flights were focused on the so-called 'wave pouch' (Dunkerton *et al.*, 2009) and its immediate vicinity. The wave pouch is defined as the region of recirculating streamlines depicted in the frame of reference at a given altitude moving with the tropical disturbance in the lower troposphere and the centre of circulation, which is roughly the location at which, according to the marsupial paradigm, a tropical cyclone is most likely to form. In the PREDICT experiment, the 700 mb level was typically used to track the pouch of a candidate disturbance and to delineate its boundary with environmental air. The data from PREDICT provide a unique opportunity to examine the evolution of the thermodynamic and kinematic structure of the wave pouches identified for both developing and non-developing systems.

In this study we will examine thermodynamic aspects of the sounding data acquired during the experiment, focusing on the day-to-day changes in the mean profiles of potential temperature and equivalent potential temperature. While these analyses cannot directly offer an understanding of the spin-up process on the mesoscale, nonetheless they offer quantitative information on the changes in the thermodynamic mean states during development or non-development, such as the stabilization or otherwise of the mean sounding and the moistening of the mean sounding during the evolution of the disturbance.

The outline of this article is as follows. Section 2 details the events discussed and section 3 describes the dropwindsonde data and methods of analysis. Section 4 presents the results of the analyses for each storm. The results are discussed in section 5 and the conclusions are given in section 6.

2. Events discussed

The storms sampled by PREDICT aircraft missions are summarized by Montgomery *et al.* (2012, their Table 2). These storms were fairly evenly split between developing and non-developing systems. While some cases had a high potential for genesis from the time of the first GV flight into them (and subsequently developed), one system departed from this pattern. *Gaston* was a surprising instance where development occurred initially but, following a period of decline (sampled by the GV and DC-8), re-development did not occur. *Matthew* formed in only three days from a weak disturbance in the mid-Atlantic Intertropical Convergence Zone (ITCZ). The main focus of this study is on the three storms: ex-tropical storm *Gaston*, pre-hurricane *Karl* and pre-tropical storm *Matthew*.

In the analyses presented, the negative ocean influence of the mixing up of cold water beneath the thermocline to the surface is neglected because the development and non-development of tropical disturbances occurs at relatively low

*The Genesis and Rapid Intensification Processes (GRIP) project of NASA and the Intensity Forecasting Experiment (IFEX) of the NOAA.

†The glossary on the NOAA Hurricane Research Division website uses tropical cyclone as 'the generic term for a non-frontal synoptic-scale low-pressure system over tropical or subtropical waters with organized convection (i.e. thunderstorm activity) and a definite cyclonic surface wind circulation'. Notably, this definition does not invoke any wind threshold. The same glossary defines a tropical depression as 'a tropical cyclone with maximum sustained surface winds of less than 17 m s^{-1} (34 kt, 39 mph) and, in the Atlantic and Eastern Pacific Basins, a tropical storm as a tropical cyclone with surface winds between 17 m s^{-1} and 33 m s^{-1}'. In this study we will define genesis as the formation of a tropical depression and we impose no formal threshold on wind speed.

‡In the Tropical Cyclone Structure 2008 (TCS08) experiment, the US Air Force C-130 aircraft was flown at a relatively high altitude of approximately 9 km in conjunction with the Naval Research Laboratory P-3 with the ELDORA radar and Doppler wind lidar on board. However, during the experiments before TCS08, flight altitudes were limited to a few km.

surface winds (approximately 30 knots or less) where the impact of wind-induced mixing of cold water is small (Shay, 2010).

3. Dropwindsonde data

Between 20 and 25 dropwindsondes were made during each GV flight mission. Diurnal cycle effects were largely filtered by the fact that the GV flights were carried out at approximately the same time of day. After quality control using the NCAR Aspen software and further manual inspection to eliminate sondes that did not record all the way to the surface, the precise number of usable sondes from the GV is summarized here. For ex-tropical storm *Gaston*: 20 on 2 September, 21 on 3 and 5 September, and 22 on 6 and 7 September. For pre-hurricane *Karl*: 21 for the two flights on 10 September and the flights on 11 and 14 September, 22 on 12 September and 20 on 13 September. For pre-tropical storm *Matthew*: 21 on 20, 21 and 24 September and 16 on 22 September. Many of these soundings were released from altitudes between 13 and 14 km, giving an unprecedented glimpse of the structure of much of the tropical troposphere in the systems studied. Radiosonde soundings from island stations at similar latitudes show that the tropopause lies around 15–16 km in the region of interest. Dropwindsonde soundings were made also by the DC8 during the last two days of ex-tropical storm *Gaston* (17 and 14 usable sondes on 6 and 7 September, respectively) and for the last three days of pre-hurricane *Karl* (18, 19 and 12 sondes on 12, 13, 14 September, respectively).

Because of safety considerations, all of the GV soundings were either in environmental air or on the periphery of convective anvils. Figure 1 shows an example of the distribution of dropsondes in relation to the wave-pouch region of the pre-*Karl* disturbance on 13 September. The convection and accompanying anvil clouds are indicated by the infra-red satellite imagery. The wave-pouch region is identified by the parent wave trough axis (black curve) and the 700 mb streamlines as viewed in the frame of reference moving with the parent wave-like disturbance (the so-called co-moving streamlines). The green curve is the local critical latitude of the parent easterly wave. The intersection between the wave trough and the critical latitude is the so-called 'sweet spot', where theory predicts that convection will ultimately organize. Indeed, this location was where the convection did organize on 14 September (Montgomery *et al.*, 2012, give further details). Figure 1 shows the planned flight track and drop points for the GV (a) and actual GV flight track (b) that had to be re-designed in real time to avoid the line of intense, deep convection oriented in a north–south configuration. In panel (b), yellow represents the GV track that is older than two hours and red represents the track that is younger than two hours. The 700 mb co-moving streamlines are shown overlaid with IR images and a lightning and 'overshooting top' product from C. Velden's group on the PREDICT science team (Figure 1 caption gives further details). The inference is that the PREDICT dropsondes were sampling the wave pouch and its near environment and not clouds *per se*.

The data from all of these soundings were interpolated to levels at intervals of 100 m above the surface. These data were then used to derive various quantities of thermodynamic interest such as the total precipitable water (TPW), Convective Available Potential Energy (CAPE) and Convective Inhibition (CIN). As is well known, CAPE is normally defined as the *maximum* kinetic energy an ascending air parcel can acquire in ascending to its level of neutral buoyancy (LNB) as a result of the vertical buoyancy force per unit mass. The calculation depends on certain assumptions. Normally, it is assumed that the parcel rises pseudo-adiabatically without mixing with its environment and the latent heat of fusion is neglected. Mixing of the rising air parcel with its environment will generally reduce its buoyancy (e.g. Stommel, 1947), but the amount of mixing is difficult to quantify with any certainty. The latent heat of fusion is neglected because the precise temperature at which freezing occurs is not known, although evidence over the tropical oceans suggests that very little liquid water remains at temperatures below –17 °C (Stith *et al.*, 2004), and freezing becomes complete at temperatures below –40 °C. To some degree, there will be compensation between these effects on the vertically integrated buoyancy in any more general definition of CAPE. In this article, we use CAPE as normally defined as a rough indication of the potential for vigorous updraughts to occur due to buoyancy, but not as a measure of actual convective vigour. Of course, buoyant updraughts cannot be realized unless the CIN is sufficiently small. The method we use for calculating CAPE and CIN is detailed briefly in the Appendix.

The DC-8 sondes were released mostly from altitudes of around 10 km, several kilometres lower than from the GV and often well below the LNB for air parcels lifted from near the surface. For this reason and the fact that CAPE and CIN values turn out to be of limited value in distinguishing between developing and non-developing systems, CAPE and CIN values were calculated only for the GV sondes.

4. Results

4.1. Ex-Gaston: 2–7 September

Tropical storm *Gaston* developed from an African easterly wave and was named by the National Hurricane Center (NHC) at 1500 UTC on 1 September. However, dropsondes from the GV deployed during its first mission into *Gaston* on 2 September indicated that the storm had weakened to a tropical depression, whereupon *Gaston* was officially downgraded to an INVEST[§]. The disturbance maintained an identity that could be tracked across the Caribbean although the convective activity weakened considerably after 7 September. Five GV flights were made into the disturbance on each day from 2 to 7 September, except on 4 September.

Figure 2 shows objective analyses[¶] of the surface pressure for each of the five flights. The flight tracks, drop points and drop times are shown also (the drop times in the right panels). In general, the fields show coherent patterns on a scale larger than the spacing between sondes, a feature that we interpret to be affirmation of the integrity of the data. One surface pressure reading at 1745 UTC on 2 September seemed suspiciously high and was replaced by an average of

[§]The term INVEST is used by operational tropical cyclone forecast centres to identify an area of interest for collection of specialized observations or running model guidance. The designation of a system as an INVEST does not correspond to a likelihood of development.

[¶]All objective analyses shown here are carried out using a bivariate interpolation method for irregularly spaced points in two dimensions using the subroutine *idbvip* written in Fortran and available from NCAR's public software library. The method is described by Hiroshi (1978, 1984).

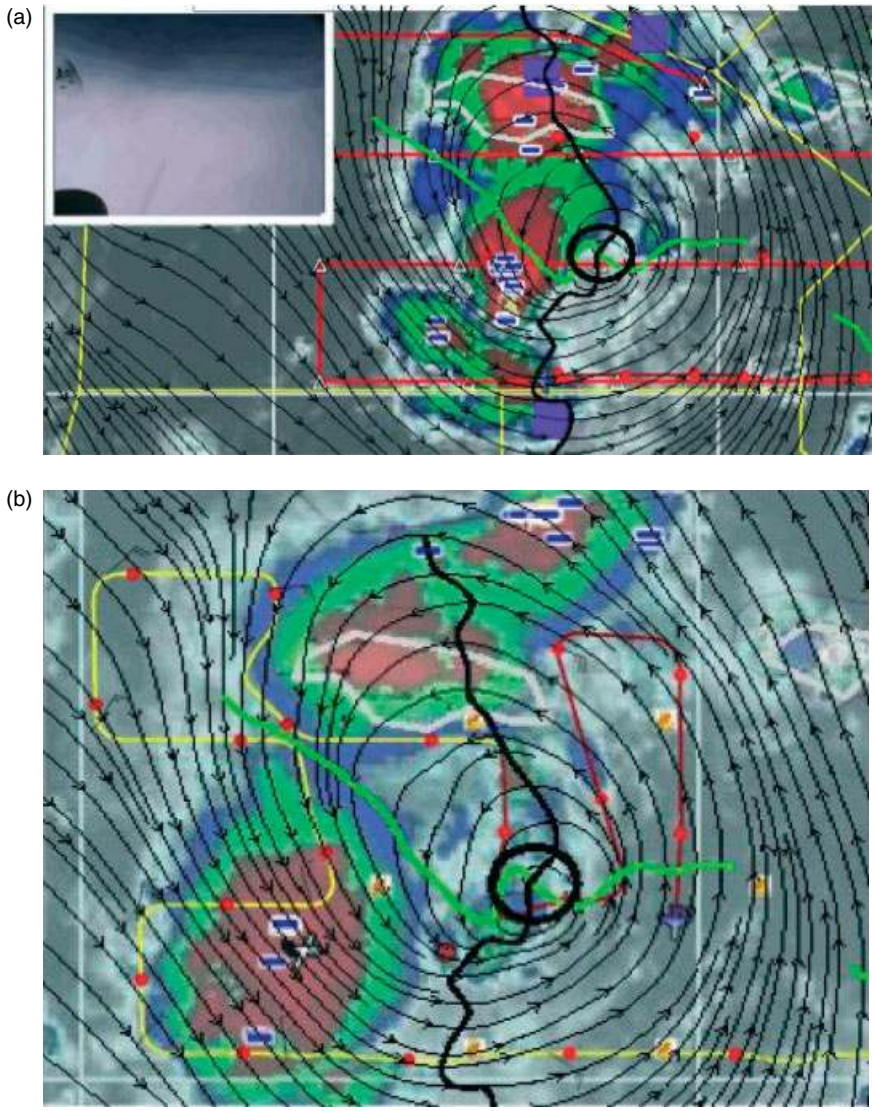

Figure 1. Illustration of forecast tools used by the PREDICT science team showing the distribution of dropsondes in relation to the wave-pouch region sampled by the GV aircraft flying between 13 and 14 km altitude. (a) shows the planned flight path (in red) of the GV within the tropical disturbance 'pre-*Karl*' on 13 September. The chosen time of the satellite image is relatively early in the flight and the aircraft location is indicated by the red aircraft symbol along the bottom flight track. Superimposed on the track is an infrared satellite image at 1137 UTC, indicating the location of deep convection (red denotes cloud tops with temperatures less than –70 °C and yellow denotes cloud tops less than –80 °C) and accompanying anvil clouds. The regions of active lightning are indicated by the horizontal blue lines and the regions of strong overshooting cloud tops are indicated by the three purple squares. The wave-pouch region is identified by both the (black) wave-trough curve and the ECMWF co-moving streamlines at 1200 UTC that re-circulate in a cyclonic sense on the 700 mb surface. The green curve is the local critical latitude of the parent easterly wave where the wave's zonal phase speed coincides with the local easterly mean flow. The inset on the upper left is a photograph taken from the remote camera on board the right wing of the GV at the position of the aircraft shown. (b) is an expanded view in format similar to (a) with the same co-moving streamline field, but with an updated satellite image at 1426 UTC. The actual flight path of the GV (yellow and red curves) was revised during the flight in order to avoid penetrating the region of vigorous deep convection (yellow in (a)) that was emerging directly ahead of the GV's track. The second aircraft symbol in this image (lower left) denotes the location of the NOAA P-3 aircraft that was flying a coordinated mission with the GV in order to sample the convective region with the airborne Doppler radar system at lower altitude of approximately 4 km. The faint yellow symbols denote successive locations of this aircraft. Other features are as described in (a). For further details see text and PREDICT science summaries available at http://catalog.eol.ucar.edu/cgi-bin/predict/report/index

those from neighbouring points at about the same latitude. Interestingly, the pressure pattern on 2 September has the appearance of a trough, whereas on subsequent days there were some closed isobars (at 0.5 mb spacing), suggesting that *Gaston* was trying to redevelop. As the main focus of this article is on the thermodynamical aspects of the systems, the relationship of the surface pressure field to the observed flow field will be discussed in a separate publication.

The right panels in Figure 2 show the corresponding distribution of TPW derived from the sondes. Satellite imagery indicated that *Gaston* was surrounded by relatively dry air during its westward transit across the Atlantic and it was speculated by forecasters that this was the reason for *Gaston*'s failure to redevelop. A Lagrangian perspective on the interaction between the dry environment and the moist pouch is presented by Rutherford and Montgomery (2011). That work documents the import of dry air into the pouch in the middle troposphere and the severing of the 'umbilical chord' of moisture from the ITCZ. For reasons articulated below, these conditions do not favour development.

The presence of dry air is confirmed by the TPW analyses and, especially on 5 September, dry air is seen to be wrapping around the southern side of the depression. Nevertheless the core, or pouch, region maintains relatively high TPW values (> 50 kg m^{-2}) throughout the period of study. Indeed, we present evidence below to show that the lowest 1 km actually

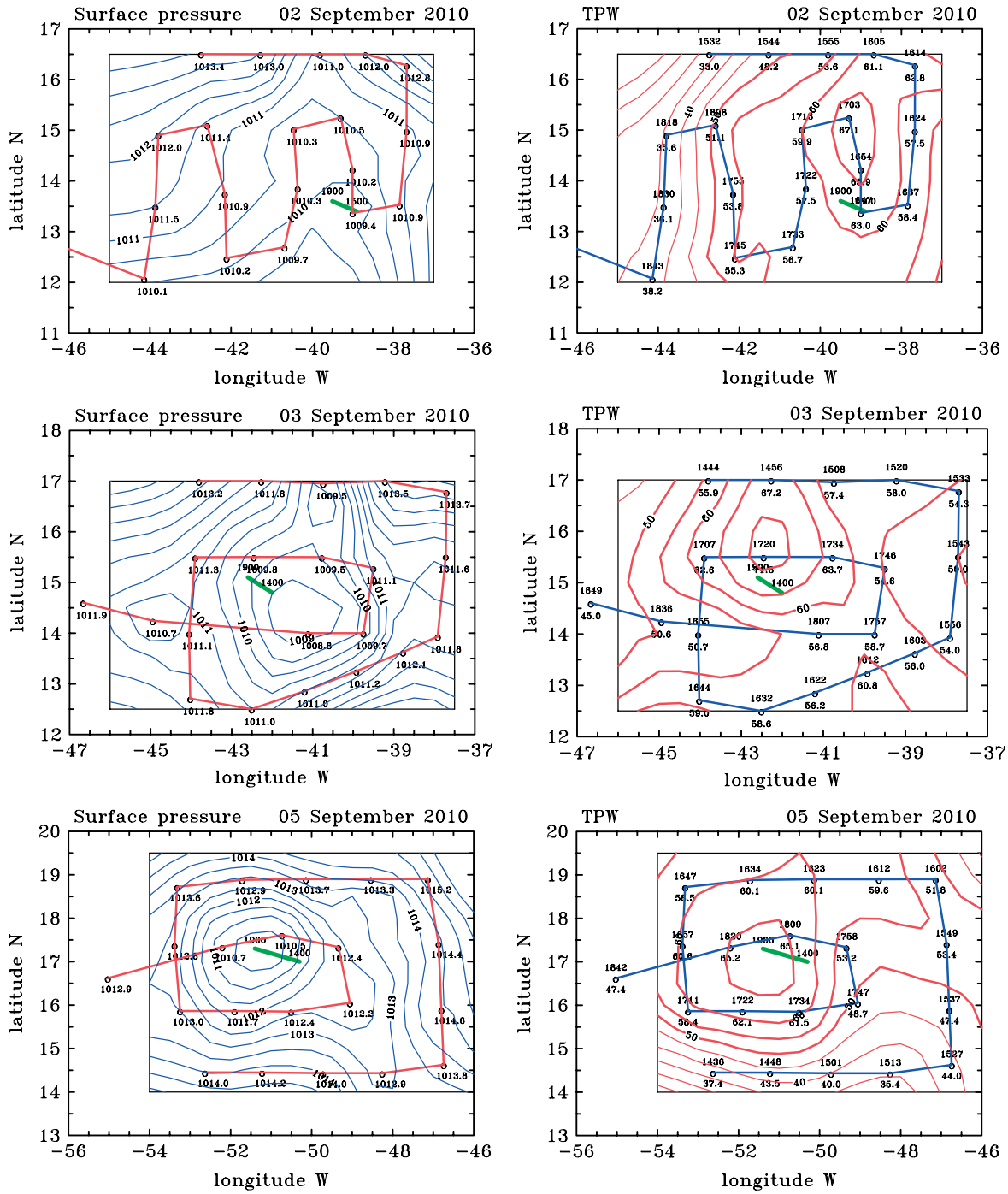

Figure 2. Objective analyses of surface pressure (left panels) and total precipitable water (right panels) for ex-tropical storm *Gaston* on 2, 3 and 5 September 2010. The contour interval is 0.5 mb for pressure and 5 kg m^{-2} for TPW. Values of TPW $\geq$ 50 kg m^{-2} are highlighted by bold contours. The aircraft track is marked with the location of soundings along the track (small circles). The data value is given below the circle and time of the sounding (UTC) is given above the circle in the TPW plots. The original surface pressure from the sounding at 1745 UTC on 2 September was suspiciously high (1015.6 mb) and was replaced by the average of the two adjacent values at 1733 UTC and 1843 UTC. The approximate track of the sweet spot during the flight with starting and ending times indicated is marked by the short bold line. Figure continued on the next page. This figure is available in colour online at wileyonlinelibrary.com/journal/qj

moistened during the five aircraft missions, although the middle and upper troposphere did not (Figure 8). It will be noted that the highest TPW values lie broadly within the region of lowest surface pressures on all days and encompass the sweet spot. Figure 3 shows frequency diagrams of TPW values from the five flights. Significantly, the percentage of *relatively high* TPW values ($\geq$ 55 kg m^{-2}) on the five days and the number of usable sondes (in brackets) were 55% (20), 67% (21), 48% (21), 33% (22) and 45% (22), respectively. It is interesting to compare these percentages with the corresponding ones for pre-hurricane *Karl* given in section 4.2, which are considerably higher.

Figure 4 shows the vertical structure of virtual potential temperature (θ_v), pseudo-equivalent potential temperature[‖] (θ_e), and saturation pseudo-equivalent potential temperature (θ_{es}) for four selected soundings on 5 September, two

[‖]The pseudo-equivalent potential temperature was calculated using Bolton's formula (Bolton, 1980).

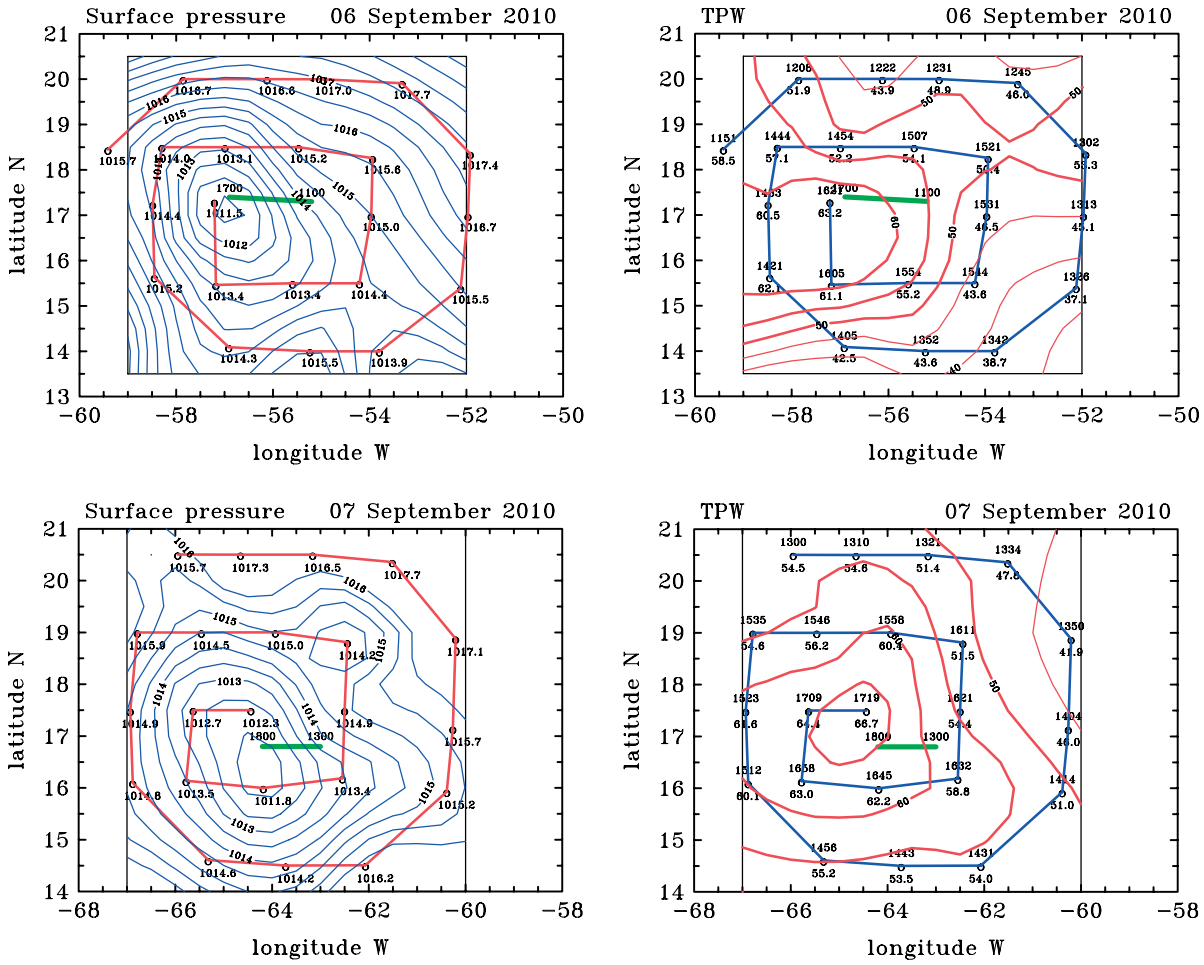

Figure 2. (continued) Objective analyses of surface pressure (left panels) and total precipitable water (TPW) (right panels) for ex-tropical storm *Gaston* on 6 and 7 September 2010. This figure is available in colour online at wileyonlinelibrary.com/journal/qj

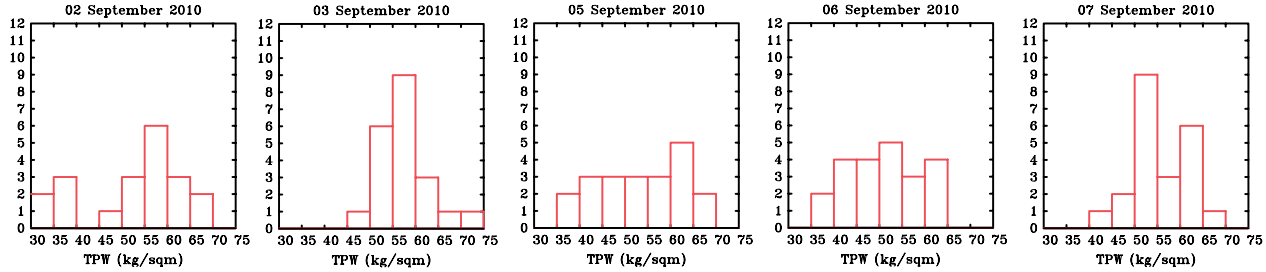

Figure 3. Frequency diagrams of TPW for ex-*Gaston* on 2, 3, 5, 6 and 7 September 2010. This figure is available in colour online at wileyonlinelibrary.com/journal/qj

in the region of highest TPW and two in the dry air to the south of this region. The vertical lines in the figure show the θ_e values for air parcels at the surface and at a height of 100 m above the surface. Since θ_e would be conserved assuming undilute ascent with or without condensation, these lines represent the θ_e of moist air parcels lifted from these levels. Moreover, the distance between the vertical line and the θ_{es} curve at a given height is roughly proportional to the buoyancy of the lifted air parcel at this height, with the buoyancy being positive when the parcel line is to the right of the θ_{es} curve. Thus, assuming undilute ascent, the first intersection of the vertical line with the θ_{es} curve is the approximate level of free convection (LFC) and the final intersection is approximately equal to the LNB for the particular air parcel (Ooyama, 1969; Emanuel, 1994; Holton, 2004). Furthermore, the area between these lines and the θ_{es} curve in the range between the LFC and LNB is roughly proportional to the CAPE and that between the surface and the LFC is roughly proportional to the CIN. The following features may be noted:

- The height from which the soundings were made was mostly close to the LNB, allowing reasonably accurate estimates of CAPE**.
- The vertical structure of θ_v shows the expected monotonic increase with height and varies little between soundings.

**In cases where the LNB was above the sounding, the sounding was extended, guided by that in the European Centre for Medium-range Weather Forecasts (ECMWF) analyses in the storm location.

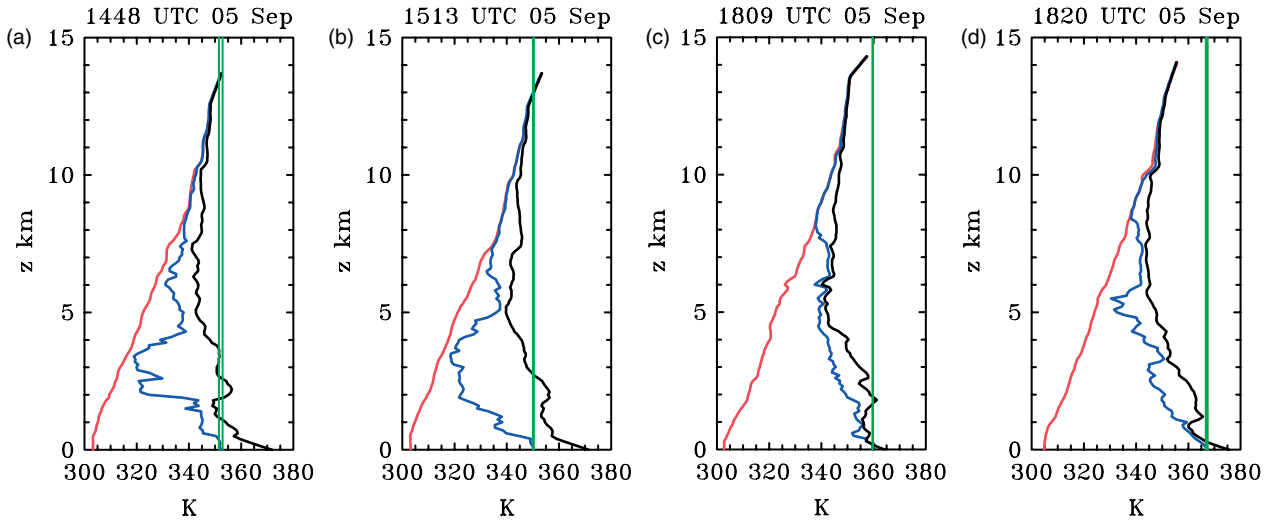

Figure 4. Four soundings for ex-*Gaston* on 5 September: (a) 1448 UTC, (b) 1513 UTC, (c) 1809 UTC, and (d) 1820 UTC. Figure 2 shows sounding positions in relation to TPW. The left curves show θ_v, the middle curves θ_e, and the right curves θ_{es}. The vertical lines show values of θ_e for air parcels at the surface and 100 m. The intersection of these lines with the θ_{es} show the approximate locations of the LFC and LNB. See text for discussion. This figure is available in colour online at wileyonlinelibrary.com/journal/qj

- The LFC of the two soundings on the southern side of the domain is relatively high and, judged directly from these figures, these soundings have considerably lower CAPE than the two moist soundings[††]. Indeed, air parcels lifted from, or near, the surface would acquire little or no buoyancy below a height of about 4 km. A striking feature of these sounding is the low values of θ_e in the low to middle troposphere, there being a large saturation deficit, as measured by $\theta_{es} - \theta_e$, exceeding 30 K. These values indicate the presence of relatively dry air at these levels.
- The LFC of the two moist soundings is much lower than the two dry ones and the CIN is correspondingly lower. Moreover, the buoyancy of lifted air parcels is much larger, whereupon the values of CAPE are much larger also. For these soundings, the saturation deficit is relatively small throughout much of the troposphere.

Figure 5 shows similar profiles of all soundings with a TPW equal to or higher than 50 kg m^{-2} together with their mean on each day of measurement[‡‡]. The foregoing criterion was found to correspond roughly with the region of closed streamline contours at 700 mb in the ECMWF analysis near the time of the mission and eliminated only a small fraction of soundings on the periphery of the system. Therefore, this value of TPW is used throughout this study as a rough proxy for the pouch.

Consistent with the four soundings shown in Figure 4, the vertical structure of θ_v shows little variability between soundings. However, there is considerable variability in the vertical structure of θ_e on a particular day. The variability between the daily-mean soundings is discussed later (Figure 8). On all days, the vast majority of the θ_e curves lie to the left of the θ_{es} curve for the mean sounding.

Figure 6 shows the spatial distribution of CAPE and CIN for the five missions into ex-*Gaston* and Figure 7 shows a scatter plot of CAPE and CIN for all soundings, identified by day. Figure 6 shows also the track segment of the sweet spot during the flight mission. The following features are evident:

- On all days there are some relatively high values of CAPE (> 1500 J kg^{-1}), with the maximum values increasing from day to day. On the last three missions, between one and five soundings have values exceeding 3000 J kg^{-1}, the most being on 7 September.
- On most days, the high CAPE and low CIN values are located in the vicinity of the minimum surface pressures, i.e. near the sweet spot.
- Soundings with high values of CAPE tend to have relatively low values of CIN (Figure 7).

The statistics of the CAPE and CIN values can be summarized by constructing frequency diagrams (not shown). The main findings are as follows:

- On 2 September, only 15% of soundings have values of CAPE exceeding 1500 J kg^{-1} and none have values exceeding 2000 J kg^{-1}. However, the CAPE broadly increased during the five days of monitoring and on 7 September, 91%, 45% and 23% of soundings have values of CAPE exceeding 1500, 2500 and 3000 J kg^{-1}, respectively.
- At least half of soundings have CIN values below 40 J kg^{-1} and between 45% and 82% had values below 20 J kg^{-1}. On 2 September, 36% of soundings have CIN values larger than 100 J kg^{-1}, while there were no such values on subsequent days.
- The largest percentage of soundings with CIN values below 40 J kg^{-1} was on 6 September (100%) and the largest percentage with values below 20 J kg^{-1} (82%) was on 6 September.

These results show that as the system evolves there is a trend towards the development of higher values of CAPE. Nevertheless, despite the increasing CAPE near the sweet

[††] Actual values of CAPE, calculated by the method given in the appendix, are shown in Figure 6.

[‡‡] The number and percentage (in brackets) of soundings with TPW > 50 kg m^{-2} was 14 (70%), 20 (90%), 14 (67%), 12 (55%), 19 (86%) on 2, 3, 5, 6, 7 September, respectively

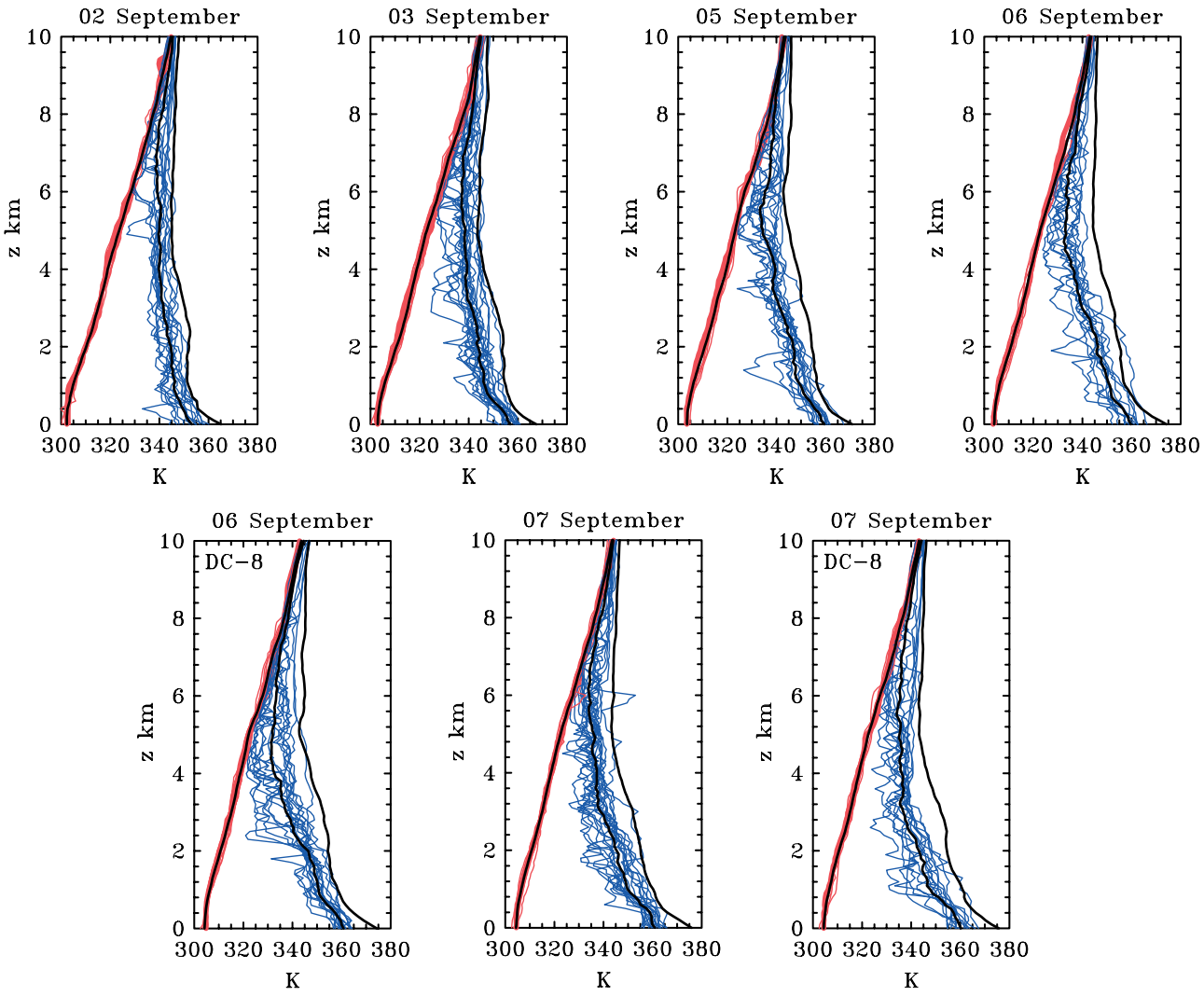

Figure 5. All soundings of θ_v (red curves) and θ_e (blue curves) for *Gaston* on 2, 3 and 5–7 September 2010 as indicated. The pouch-means of θ_v, θ_e are indicated by black curves. The right black curve is the θ_{es} for the pouch-mean sounding. The lower left and right panels show soundings from the NASA DC-8 flights on 6 and 7 September.

spot, the system did not redevelop over the five days of measurements. Evidently, these metrics by themselves are insufficient indicators of the failure of the system to redevelop.

Figure 8 shows the day-to-day evolution of the 'pouch-mean' soundings obtained from the dropsondes during missions into ex-*Gaston*. These pouch-mean soundings are characterized by θ_v and θ_e as functions of height. Figure 8(b, c) shows the deviations of θ_v and θ_e from the five-day mean. Features that stand out are:

- There is only a slight difference in the day-to-day variation in the system-average θ_v.
- There is a monotonic warming of θ_v in the lowest 2 km, exceeding 2 K near the surface. Above 3 km altitude, there is cooling on the order of 1 to 1.5 K at all heights up to at least 10 km.
- There is a general day-to-day increase in the lower tropospheric θ_e, but at mid-upper levels ($z > 3$ km), the mean θ_e decreases with time.
- There is a relatively large difference (typically 25 K) between near-surface θ_e value and those of the mid-troposphere minimum.

It is reasonable to speculate that the warming and at least part of the increase in θ_e at low levels is due to the increase in sea-surface temperature (about 1 °C) as ex-*Gaston* moved across the Atlantic Ocean and then over the warmer Caribbean Sea.

Traditional reasoning would suggest that ensuing convection within a relatively dry, elevated layer of air would lead to comparatively strong downdraughts (e.g. Emanuel, 1994). From the perspective of convective dynamics, stronger downdraughts (implied by the lower relative humidity at heights between about 2 and 8 km in *Gaston* inferred from the θ_e profiles in Figure 8(a) and 8(c)) would tend to import low θ_e into the boundary layer and frustrate the enhancement of boundary-layer θ_e by sea-to-air moisture fluxes. This enhancement is necessary to fuel subsequent deep convective activity. However, recent numerical modelling studies by James and Markowski (2009) and Kilroy (2011, personal communication) suggest that the principal effects of the dry air are to reduce the convective updraught strength and water loading, while the convective downdraught strengths are not changed appreciably. The dilution of the updraught with dry air would reduce cloud buoyancy, making the updraught less effective in amplifying vertical vorticity throughout a significant depth (section 5).

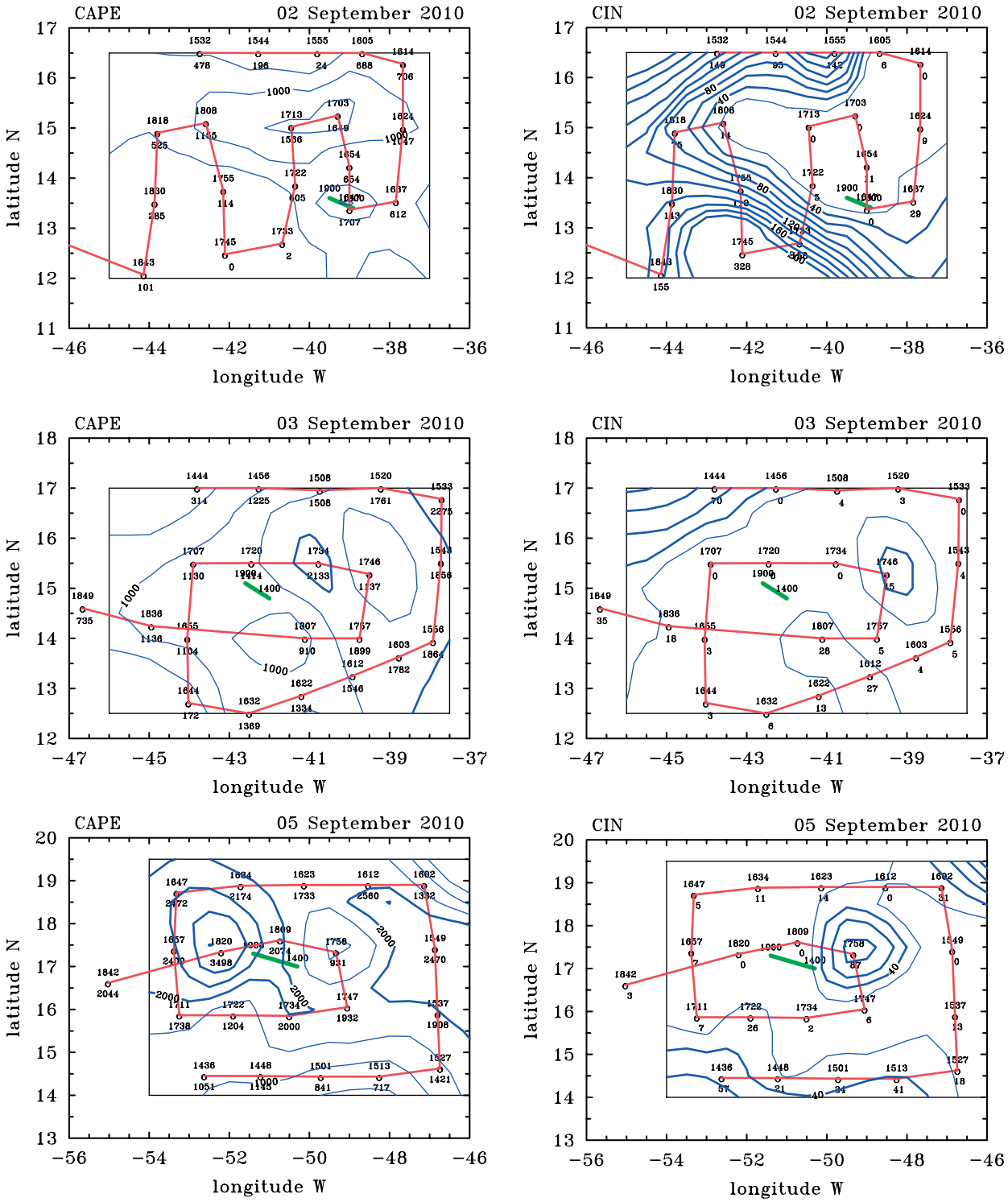

Figure 6. Objective analyses of CAPE (left panels) and CIN (right panels) for ex-TS *Gaston* on 2, 3 and 5 September 2010. The contour interval for CAPE is 500 J kg^{-1}, with contours $\geq$ 2000 J kg^{-1} in bold. The contour interval for CIN is 20 J kg^{-1}, with contours $\geq$ 40 J kg^{-1} in bold. The aircraft track is marked with the location of soundings along the track (small circles). The time of the sounding (UTC) is given above the circle and the data value below the circle. The approximate track of the pouch centre during the flight with starting and ending times indicated is marked by the short bold line. Figure continued on the next page. This figure is available in colour online at wileyonlinelibrary.com/journal/qj

A recent study of tropical convection by Fierro *et al.* (2012) indicates that much of the dilution occurs in the first 2–3 km, where almost all tropical oceanic soundings show a sharp decrease in θ_e with height. As emphasized, the foregoing remarks apply strictly to the convective scales and not to mesoscale dowdraughts associated with regions of stratiform precipitation. Nevertheless, James and Markowski (2009) found that in quasi-linear convective systems, the mesoscale downdraught and cold pool strengths were enhanced only in high CAPE ($>$ 3000 J kg^{-1}) situations.

As to the source of this drier air in ex-*Gaston*, there is evidence of a dry air mass surrounding the northern hemisphere of ex-*Gaston* in multiple satellite-derived products. A Lagrangian analysis carried out by Rutherford and Montgomery (2011) indicates strongly that the dry air seen in the observations is the result of a complex process of

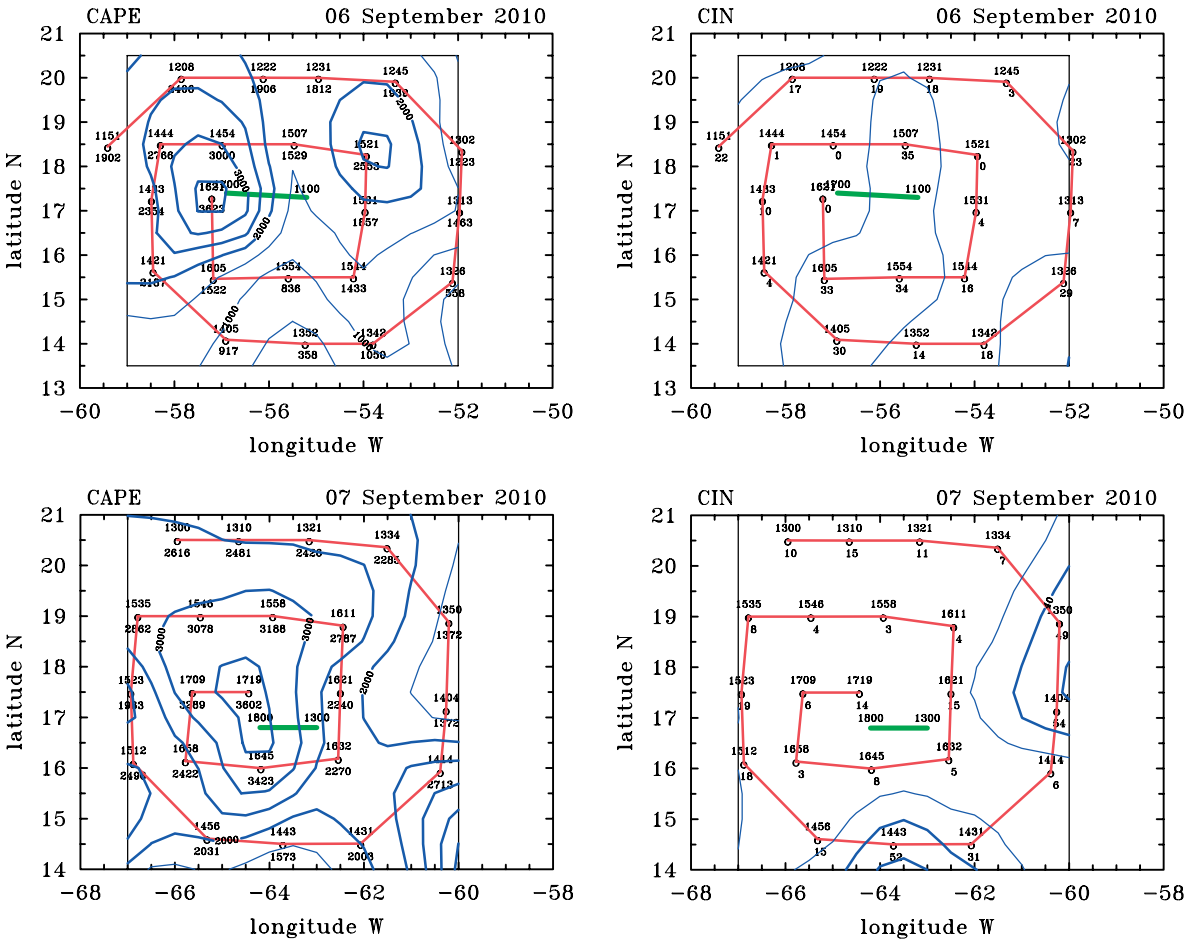

Figure 6. (Continued) Objective analyses of CAPE (left panels) and CIN (right panels) for ex-TS *Gaston* on 6 and 7 September 2010. This figure is available in colour online at wileyonlinelibrary.com/journal/qj

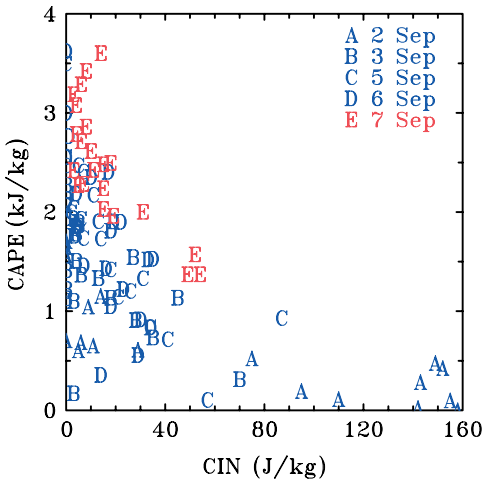

Figure 7. Scatter plot of CAPE and CIN values for the 106 soundings in ex-*Gaston*. Note the tendency for soundings with high CAPE to have low CIN. This figure is available in colour online at wileyonlinelibrary.com/journal/qj

intrusion of dry air from outside of the pouch region. Dry air continued to plague ex-*Gaston* during the subsequent days. The cyclonic circulation became shallower over time also (Davis and Ahijevych, 2012; Boothe, personnal communication). By 5 September, the circulation was not evident at 500 mb and by 7 September it was barely evident at 700 mb. The storm continued to produce intense convection intermittently throughout the period, but the vortex systematically weakened.

4.2. *Pre-hurricane Karl: 10–14 September*

The disturbance that ultimately became hurricane *Karl* originated within the ITCZ region near the northern coast of South America. A surge of southwesterlies over northern South America around 8 September was accompanied by the formation of a quasi-persistent area of convection along the ITCZ near the northern coast of the continent. An easterly wave formed subsequently near this locale and propagated westwards towards the eastern Caribbean. Convection within the early pre-*Karl* disturbance was elongated east–west on 10 September. On this day, two missions were conducted, one centred on roughly 1300 UTC, the other about 6 h later. Both flights revealed a broad cyclonic wind gyre of diameter roughly 400 km, which featured similar tangential winds between 950 mb and 700 mb (Boothe, personnal communication). Pre-*Karl* was rather slow to develop over the next several days. Over the course of 11–14 September, convective activity consolidated from an initial southwest–northeast elongation to a more compact pattern encircling the sweet spot within the pouch, the latter being close to the location where *Karl* formed later on 14 September.

Figure 9 shows objective analyses of the surface pressure for the first two flights, on 10 September, and the last two on 14 September. As in Figure 2, the flight tracks, drop points

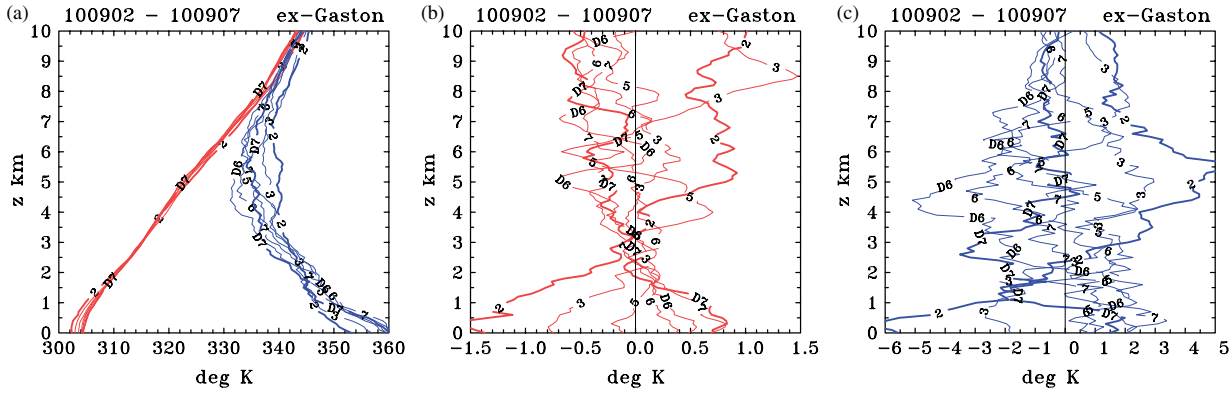

Figure 8. Vertical profiles of (a) θ_v and θ_e, and of daily departures from mean profiles for all days of (b) θ_v and (c) θ_e for ex-tropical storm *Gaston* on 2, 3, 5, 6, 7 September 2010. The bold curves mark the first and last days of the GV flights, and the number on each curves shows the date. Curves for the NASA DC-8 flights on 6 and 7 September are denoted D6 and D7, respectively. This figure is available in colour online at wileyonlinelibrary.com/journal/qj

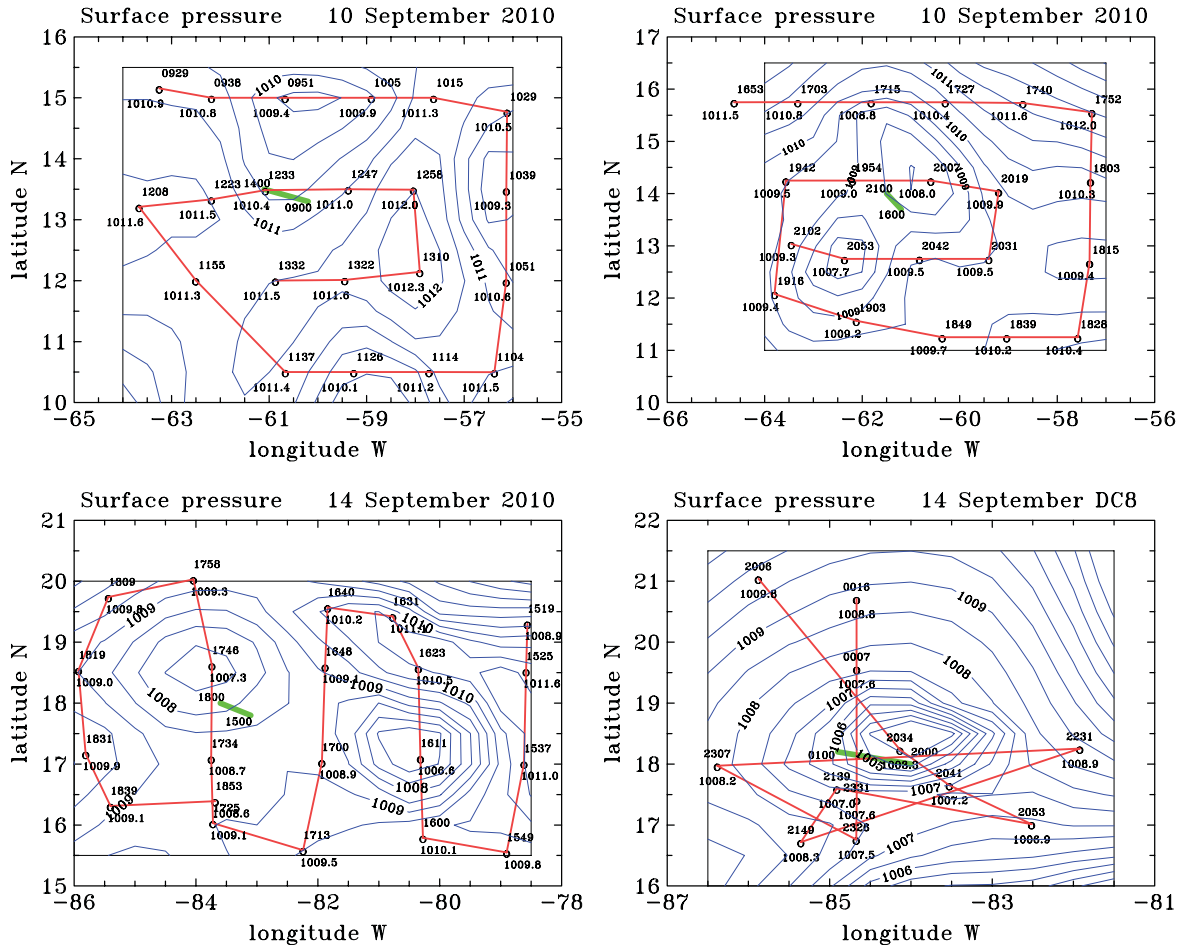

Figure 9. Objective analyses of surface pressure for the two GV flights into pre-hurricane *Karl* on the first day of observations (10 September) and the two flights on the last day (14 September), the last one being the DC-8 flight. The pressure contour interval is 0.5 mb. The aircraft track is marked with the location of soundings along the track (small circles), the data are given below the circle and the times above the circle. The approximate track of the pouch centre during the flight with starting and ending times indicated is marked by the short bold line. This figure is available in colour online at wileyonlinelibrary.com/journal/qj

and drop times are shown also, together with the track of the sweet spot during the flight. On 12 September, the flight tracks as well as the location and timing of dropsondes were unsuitable for objective analysis. As in the case of ex-*Gaston*, the analyses show coherent patterns on a scale larger than the spacing between sondes. However, unlike ex-*Gaston*, the pressure patterns from the analyses show multiple centres with closed isobars as late as the first GV mission on 14 September, approximately 6 h prior to the disturbance being declared a tropical storm. Although the later flight by the NASA DC-8 found a single pressure minimum at the surface (cf. Figure 9(d)), we caution that this minimum is based on only one sounding.

Only three soundings (all on 13 September) had values of TPW less than 50 kg m^{-2}, while 50% of soundings had values exceeding 60 kg m^{-2}, compared with only 26% for *Gaston*. For this reason, plots of TPW are not shown for *Karl*. However, we note that, as in *Gaston*, the highest TPW values

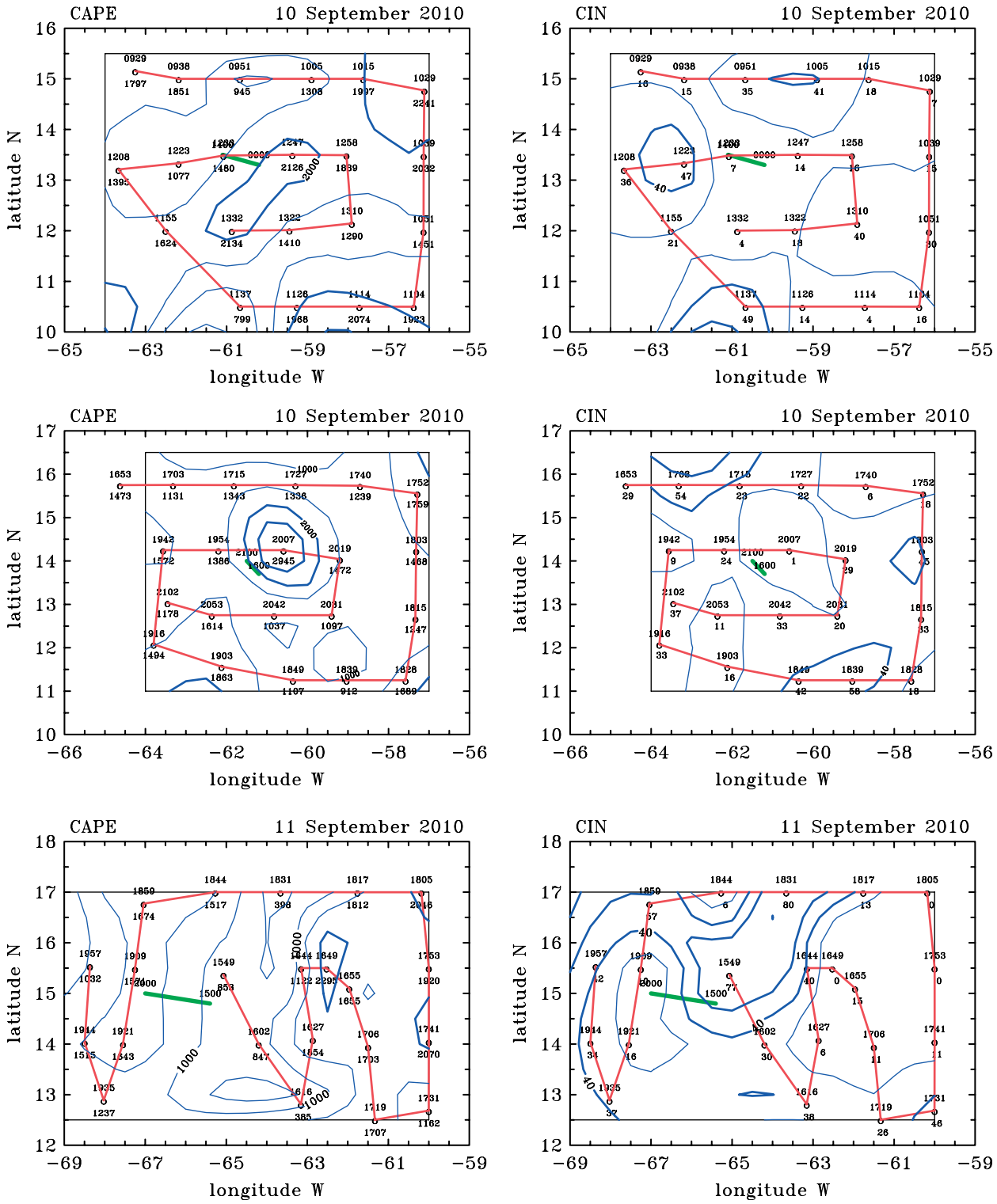

Figure 10. Objective analyses of CAPE (left columns) and CIN (right columns) for pre-hurricane *Karl* on 10 and 11 September 2010. There were two flights on 10 September. The contour interval for CAPE is 500 J kg^{-1}, with contours $\geq$ 2000 J kg^{-1} in bold. The contour interval for CIN is 20 J kg^{-1}, with contours $\geq$ 40 J kg^{-1} in bold. The aircraft track is marked with the location of soundings along the track (small circles). The time of the sounding (UTC) is given above the circle and the data value below the circle. The approximate track of the pouch centre during the flight with starting and ending times indicated is marked by the short bold line. Figure continued on the next page. This figure is available in colour online at wileyonlinelibrary.com/journal/qj

lay broadly within the region of lowest surface pressures on all days.

Figure 10 shows the spatial distribution of CAPE and CIN for the two flights on 10 September and the flights on 11, 13 and 14 September. The corresponding scatter plot for these data analogous to that shown for ex-*Gaston* (Figure 7) are shown in Figure 11. Like ex-*Gaston*, on all days there are some relatively high values of CAPE. The higher values of CAPE have relatively low values of CIN. However, unlike ex-*Gaston*, there there are no values of CAPE exceeding 3000 J kg^{-1}. There was a slight increase in the percentage of sondes having CAPE values larger than certain thresholds (see below). Furthermore, the highest values of CAPE are not near the sweet spot position.

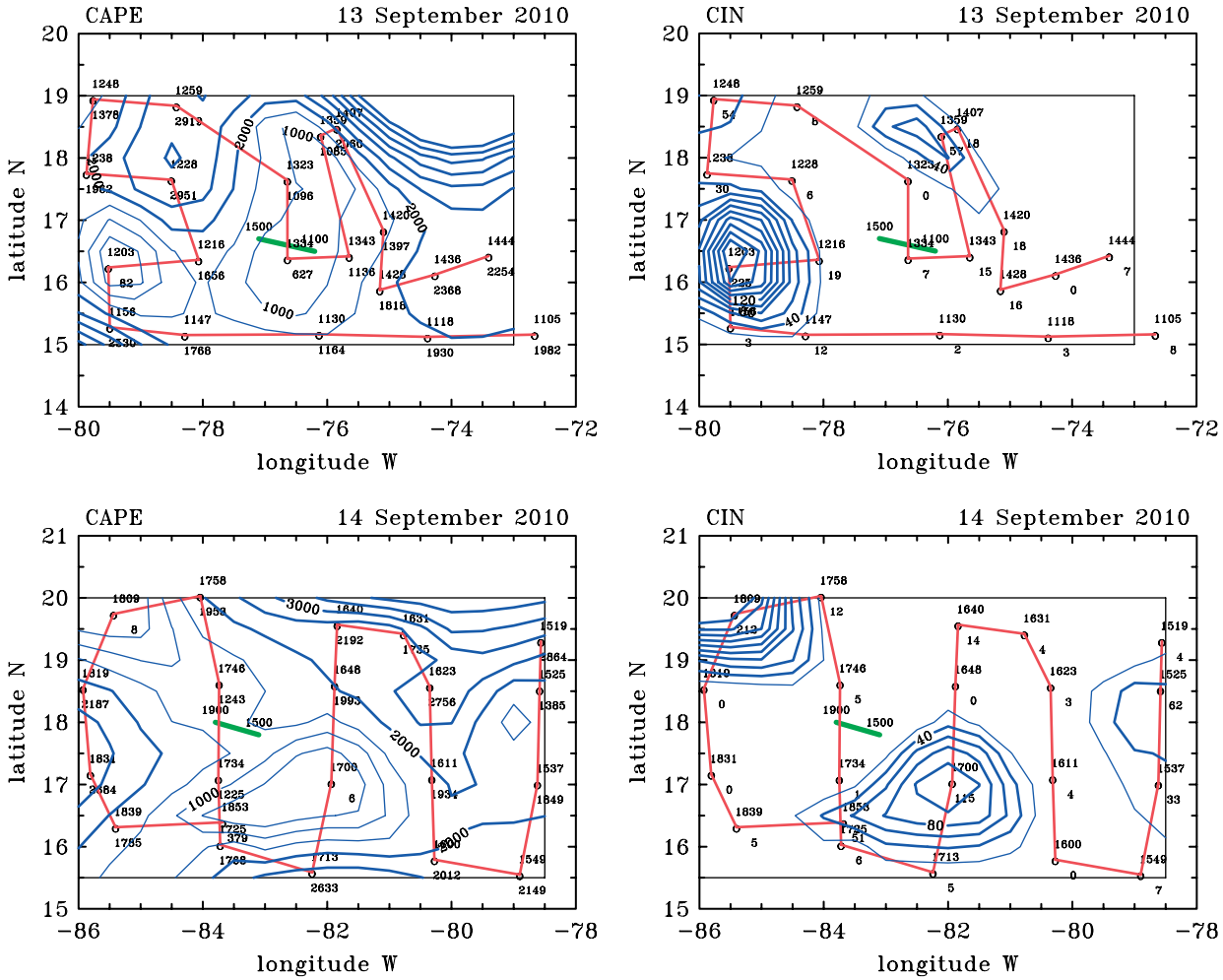

Figure 10. (continued) Objective analyses of CAPE (left columns) and CIN (right columns) for pre-hurricane *Karl* on 13 and 14 September 2010. This figure is available in colour online at wileyonlinelibrary.com/journal/qj

Some statistics can be derived also from these data using frequency diagrams (not shown):

- Discounting the CAPE values from the second flight on 10 September, which was made at a different time of day from the others, between 57% and 71% of soundings over the GV missions have values of CAPE exceeding 1500 J kg^{-1} and between 14% and 19% of soundings on the last three days have values exceeding 2500 J kg^{-1}, the largest percentages being on 14 September.
- Between 71% and 85% of soundings have values of CIN below 40 J kg^{-1} and between 33% and 80% have values below 20 J kg^{-1}, the largest percentages of the latter being on 13 September (80%) and 14 September (76%).

Figure 12 shows profiles of all soundings with a TPW $\geq$50 kg m^{-2} together with their mean on each day of measurement in pre-*Karl*. As in the case of ex-*Gaston*, the soundings are characterized by the vertical profiles of θ_v and θ_e. The main points to note are that there is little variation between soundings for θ_v and the scatter in θ_e is visually less than that in Figure 5. In addition, the vast majority of the θ_e curves lie to the left of the θ_{es} curves for the mean sounding.

Figure 13(a) shows the day-to-day evolution of the pouch-mean soundings obtained from the dropsondes. Figure 13(b, c) show the deviations of θ_v and θ_e from the five-day mean. Features that stand out are:

- As for ex-*Gaston*, there is little difference in the day-to-day variation in the system-average θ_v.
- There is a general day-to-day increase in the lower tropospheric θ_e. However, unlike the case of ex-*Gaston*, the mean θ_e at mid-upper levels ($z > 3$ km) increases over the period of observation, but this increase is not monotonic.
- There is a systematic warming of the entire troposphere between 10 and 14 September. Between the surface and 5 km altitude the warming is on the order of 0.7 K. Above 5 km, the warming increases with height and exceeds 3 K above about 9 km altitude.
- There is only a modest difference ($\sim$15 K) between the near-surface θ_e and the mid-tropospheric minimum. This is in contrast to the $\sim$25 K difference in the non-developing ex-*Gaston*.

4.3. *Pre-Matthew: 20–24 September*

In contrast with *Karl*, *Matthew* was generally unforeseen as few as 5 days prior to its formation. While the PREDICT team was tracking weak vorticity features connected with the ITCZ on 17 and 18 September, it was not until deep convection erupted on 19 September that there was a feature sufficiently defined in the atmosphere and in global models

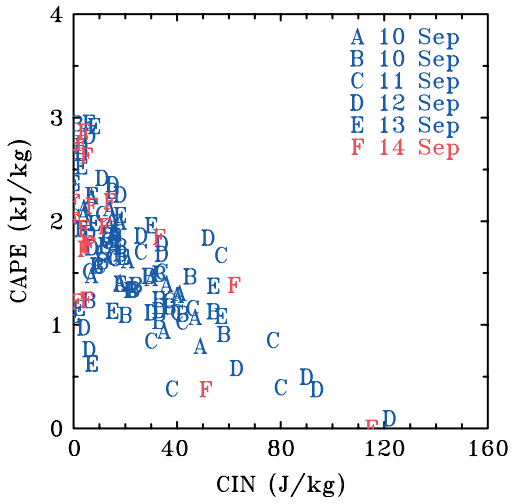

Figure 11. Scatter plots of CAPE and CIN values for the 106 soundings in pre-*Karl*. Note the tendency for soundings with high values of CAPE to have low values of CIN. This figure is available in colour online at wileyonlinelibrary.com/journal/qj

to plan a mission. The first GV mission was centred roughly on 1600 UTC on 20 September. At this time, the pre-*Matthew* disturbance appeared less organized than *Karl* when it was first flown. However, *Matthew* quickly organized on 21 and 22 September.

The pouch was well defined on 22 September with strong convection occurring close to the predicted maximum in Okubo–Weiss parameter in the analysis from the ECMWF model (Montgomery *et al.* (2012) give details). *Matthew* went on to develop into a strong tropical storm on 23 September but, despite forecasts of potential rapid intensification, it did not intensify further and made landfall in Belize as a moderate tropical storm late on 24 September. Although it had similarities to *Karl* in its mid-ocean origin and track through the Caribbean, *Matthew* developed rapidly, but failed to become a hurricane.

Figure 14 shows a scatter plot of CAPE against CIN for the GV soundings obtained in *Matthew*. Unlike the case of pre-*Karl* and ex-*Gaston*, CAPE values are generally largest on the first day of observation (20 September) with 52% soundings having CAPE exceeding 1500 J kg^{-1}: this percentage declined to 19% on 21 September and only 14% on 24 September. There is only one value of CAPE exceeding 2500 J kg^{-1} and that occurs on 20 September. The highest percentages of CIN values less than 20 J kg^{-1} and less than 40 J kg^{-1} are on 20 September (76% and 90%, respectively). These percentages decline monotonically over the next two days to 19% and 44%, respectively, and then resurge on 24 September to 48% and 71%, by which time the disturbance had been declared a tropical storm. As in the case of ex-*Gaston* and pre-*Karl*, the evolution of CAPE and CIN do not appear to provide clues to the possibility of development or non-development.

Figure 15(a) shows the day-to-day evolution of the pouch-mean soundings obtained from the dropsondes. Figure 15(b, c) show the deviations of θ_v and θ_e from the four-day mean. Features that stand out are:

- As for ex-*Gaston* and pre-*Karl*, there is little difference in the day-to-day variation in the system-average θ_v.
- Unlike ex-*Gaston* and pre-*Karl*, there is an overall increase in the lower tropospheric θ_e over the four days of observation, but the θ_e initially decreases and then increases. There is little difference in the mean θ_e over the first three days at mid-upper levels ($z > 3$ km), but over the next two days the θ_e increases by approximately 2 K. Initially, there is only a modest difference (~15 K) between the near-surface θ_e and the mid-tropospheric minimum. This difference is similar to that found in *Karl*.
- Between 20 and 21 September there is a slight cooling in θ_v below an altitude of 6 km of approximately 1 K. On subsequent days there is a systematic warming on the order of 1.5 K.
- Like θ_v, the deviation of θ_e from the five-day mean below 2 km altitude falls about 4 K. Above this altitude, there is no appreciable change up to 22 September, after which there is a systematic increase of approximately 2 K.

5. Discussion and interpretation

Over the years, the life cycle of individual deep convective clouds has been well documented and there have been text books written on the subject (e.g. Cotton and Anthes, 1989; Emanuel, 1994; Houze, 1993). It is known that such clouds have a lifetime of an hour or less. During their developing phase, they remove moist air from the lowest 1–2 km and carry it into the upper troposphere. As their updraughts become loaded with liquid water and/or ice, the lower part of the updraught decays and becomes a downdraught. The downdraught is driven by the collective drag of precipitation and, below cloud base, also by the cooling of air resulting from the evaporation of the precipitation as it falls through unsaturated air. The collective effect of downdraughts is to spread a thin carpet of cool air near the surface that tends to stabilize the air to subsequent convection. Mixing and detrainment from a spectrum of convective cells with air in the cloud environment leads to a moistening of the environment in middle and upper levels.

The traditional argument has been that downdraughts tend to be stronger when the middle-layer air in the cloud environment is dry, but, as discussed in section 4.1, this view has been challenged recently. There it was argued that the failure of *Gaston* to redevelop was traceable to the injection of dry air into *Gaston*'s pouch in the lower to middle troposphere. If the foregoing mechanisms are operating, the implications of this dry air would be a cooling and drying of the near-surface air. However, precisely the opposite is observed! In particular, the boundary-layer θ_e increased progressively over the entire observation period and yet the system did not develop. While the failure to develop may have been in part due to increasing vertical shear (Davis and Ahijevych, 2012, pers. comm.; Rutherford, 2012, pers. comm.), these findings raise a basic question: what are the consequences of the dry air on the ability of the clouds to amplify the background rotation?

When convection occurs in an environment of non-zero vertical vorticity, basic fluid dynamical considerations suggest that updraughts would amplify the vorticity by the process of vortex-tube stretching. Even for background rotation rates as low as that of an undisturbed tropical atmosphere away from the Equator, cloud model simulations confirm this tendency to amplify ambient vorticity on time scales of an hour (Saunders and Montgomery, 2004; Wissmeier and Smith, 2011). A striking

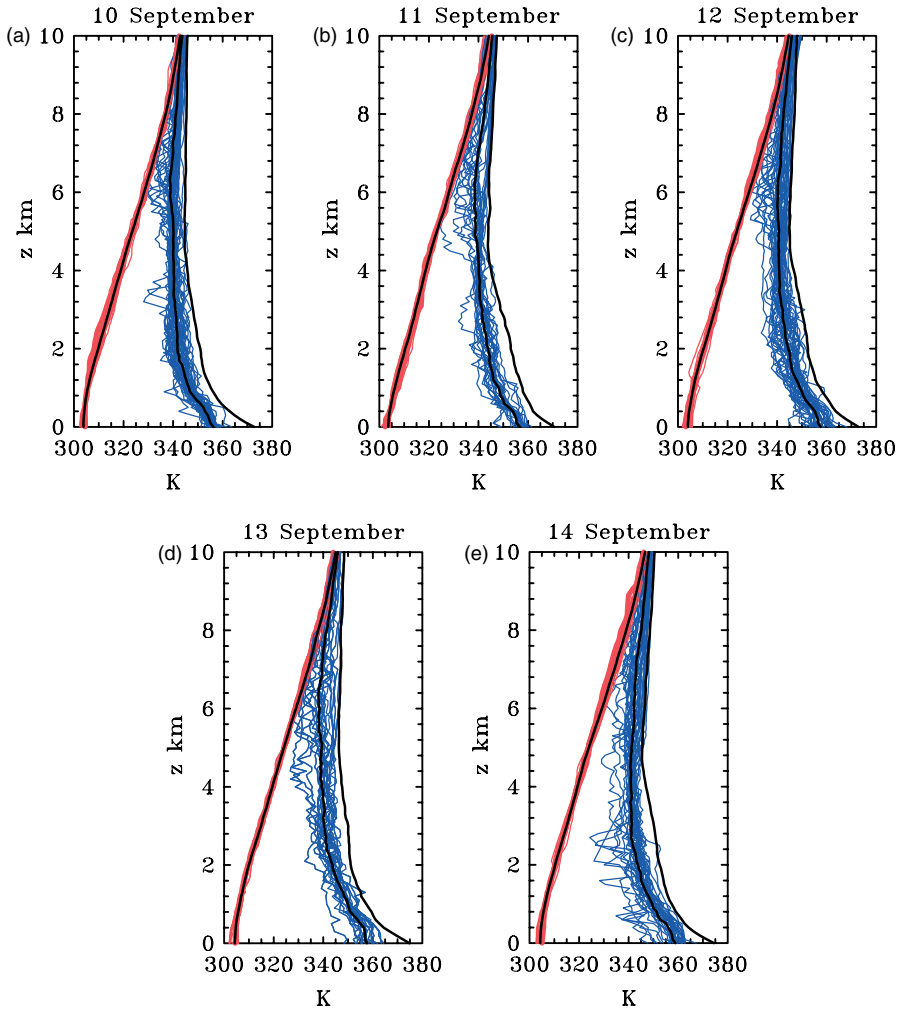

Figure 12. All pouch soundings of θ_v (red curves) and θ_e (blue curves) for pre-*Karl* on 10–14 September 2010 as indicated. The pouch means of θ_v, θ_e are indicated by black curves. The right black curve is the θ_{es} for the pouch-mean sounding. (a) contains data for both flights on 10 September, while (c), (d), (e) include both the GV and NASA DC-8 data.

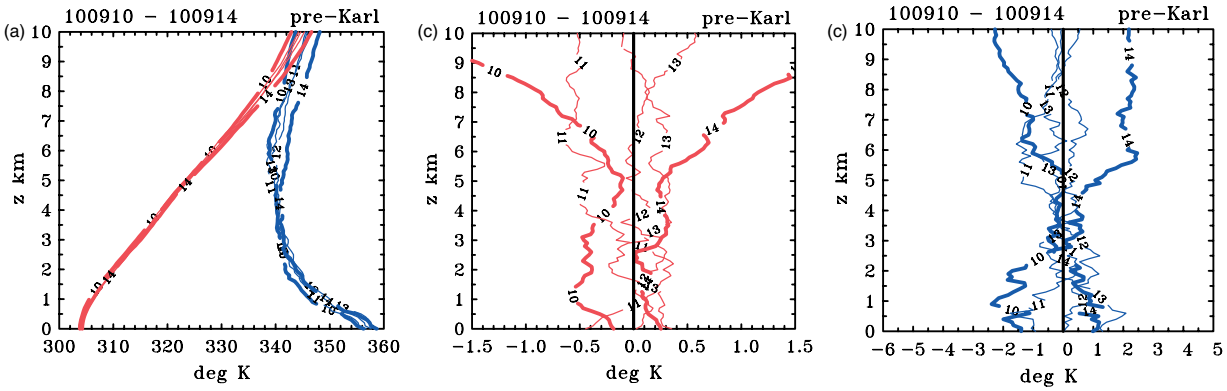

Figure 13. Vertical profiles of (a) θ_v and θ_e, and of daily departures from mean profiles of (b) θ_v and (c) θ_e for all days for pre-hurricane *Karl* on 10–14 September 2010. The bold curves mark the first and last days of the sequence, and the number on each curves shows the date. The profiles on 10 September include both GV flights, and those for 12–14 September include both GV and DC-8 data. This figure is available in colour online at wileyonlinelibrary.com/journal/qj

result of such simulations is that the amplification is between one and two orders of magnitude and is a maximum at low levels. Moreover, the enhanced vorticity persists long after the initial updraught has decayed. These cloud model simulations indicate also that the induced tangential wind speeds by a single updraught is typically no more than a few meters per second with a horizontal scale of around 1 km, and would be barely detectable by normal measurement methods in the presence of an ambient wind field. Together these results suggest that all non-shallow tropical convection away from the equator is vortical to some degree. It is not hard to imagine, then, that the stretching of vertical vorticity by a developing cumulus cloud is a fundamental process that may be an important process in tropical cyclogenesis.

Vortical convective clouds have been identified as fundamental building blocks during both the tropical

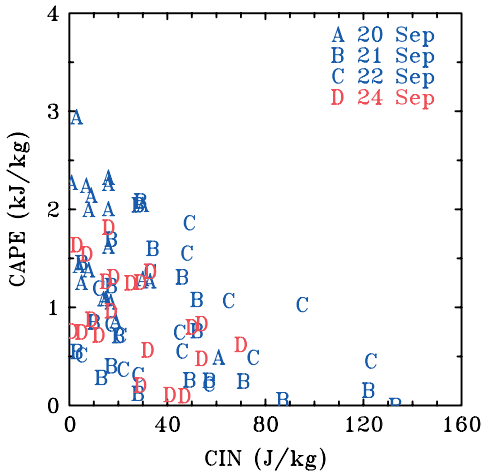

Figure 14. Scatter plot of CAPE and CIN values for the 79 soundings in pre-*Matthew*. This figure is available in colour online at wileyonlinelibrary.com/journal/qj

cyclone genesis and intensification process (Hendricks *et al.*, 2004; Montgomery *et al.*, 2006; Nguyen *et al.*, 2008; Braun *et al.*, 2010; Fang and Zhang, 2010). The vertical vorticity that is generated by the clouds outlives the convection that produced them in the first place. The like-signed vortical remnants tend to aggregate in a quasi two-dimensional manner with a corresponding upscale energy cascade, and some of these remnants will be intensified further by subsequent convective episodes. If the disturbance-scale circulation strengthens, they will tend to become axisymmetrized by the associated angular shear flow. In addition, system-scale inflow forced by the aggregate latent heating from the convective elements leads to an inward advection of convectively enhanced vorticity. Stokes' theorem applied to a fixed area *surrounding the convection* implies that there will be an accompanying increase in strength of the disturbance-scale circulation on account of the import* of ambient absolute vorticity into it. When applied to a fixed area *within the convective region*, the import of convectively enhanced vorticity into the area will lead also to an increase in the circulation. As the circulation progressively increases in strength, there is some increase in the surface moisture fluxes. However, it is not necessary that the moisture fluxes continue to increase with surface wind speed (Montgomery *et al.*, 2009). This research forms the basis of a unified view of tropical cyclogenesis and intensification (Montgomery and Smith, 2011). In this view, the separate stages proposed in previous significant studies and reviews (e.g. Frank, 1987; Emanuel, 1989; McBride, 1995; Karyampudi and Pierce, 2002; Tory and Frank, 2010) are unnecessary.

Another line of research on tropical cyclogenesis emerged from TEXMEX†. This research emphasized the importance of thermodynamical processes within the so-called 'mesoscale convective vortex embryo'. Bister and Emanuel (1997) proposed that the development of a cool, moist environment resulting from stratiform rain serves as the incubation region for the formation of a low-level, warm-core cyclonic vortex. They suggested *inter alia* that sustained precipitation in the stratiform cloud deck, together with the evaporation of rain drops below, would gradually cool and saturate the layer below cloud base while advecting cyclonic vorticity downwards to the surface. Some questions about the dynamics of this process have been raised by Tory and Montgomery (2007), but the thermodynamical aspects are interesting also and worthy of investigation using the data analysed in section 4.

In the pouch-mean data presented for the two developing storms (Figures 13 and 15), we do not find cooling of air below 10 km in altitude. Rather, *in all cases there is slight warming*.

Figure 16 shows the day-to-day evolution of the system-mean relative humidity for pre-*Karl* and pre-*Matthew*. In both disturbances there was no significant change in this quantity below about 3 km, but there was a clear moistening above this level between the first and last flight into the storm. These findings do not provide unequivocal support for the Bister and Emanuel picture described above. For one thing, we do not see a progressive increase in low- to mid-troposphere relative humidity in all cases. Furthermore, the moistening that we do see cannot be explained by evaporative cooling as it occurs in the presence of increasing temperature; it occurs also through a significant depth of the atmosphere, not just below cloud base. Of course, there is the issue of the horizontal scale differences between the data gathered during TEXMEX and those collected during PREDICT. The sampling strategy for TEXMEX was focused on the scale of a single mesoscale convective system and its associated mesoscale convective vortex, while that for the PREDICT experiment focused on the broader-scale aspects of genesis.

Influenced by the TEXMEX study, Raymond and Sessions (2007) proposed an alternative model for tropical cyclogenesis that is linked with the gross moist stability of the tropical atmosphere. They investigated the hypothesis that an increase in the gross moist stability would lead to a fundamental change in the vertical profile of convergence for a developing tropical disturbance. To this end, they carried out a series of two-dimensional (zonal–height) cumulus ensemble simulations in the context of the weak temperature gradient approximation without background rotation. The experiments imposed small thermal and moisture perturbations to a state of radiative-convective equilibrium as a possible way of investigating the evolution of convection in thermodynamic environments conducive for tropical cyclogenesis. Environments that were cooler than the radiative-convective equilibrium state at low levels and warmer at upper levels on the order 1 K (implying a more stabile column) were found to lower the level of maximum vertical mass flux from 10 km to approximately 5 km. Such environments were found to increase the precipitation rate as well. The net result of the stabilization was to concentrate the inflow into a shallow layer in the lower troposphere. Furthermore, they found that the stabilization was more effective than the moistening of a column in fostering low-level convergence. The implication is that, if realistic values of ambient rotation associated with a tropical wave or monsoon trough were included, this convergence would import sufficient absolute vorticity to overcome that lost to the surface by friction. If maintained, the net import of

*The stretching and thereby amplification of ambient (or system-scale) vorticity by convection by itself does not lead to an increase in the circulation because stretching leads to a contraction in the areal extent of the amplified vorticity (Haynes and McIntyre, 1987).

†The Tropical Experiment in Mexico (TEXMEX) was conducted in the eastern Pacific basin out of Acapulco, Mexico (Bister and Emanuel, 1997; Raymond *et al.*, 1998).

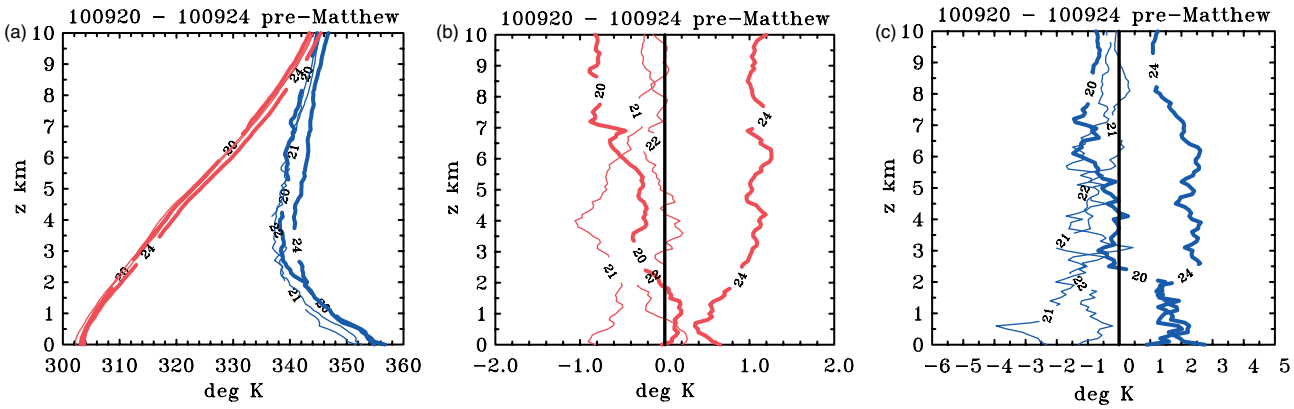

Figure 15. Vertical profiles of (a) θ_v and θ_e, and daily departures from mean profiles of (b) θ_v and (c) θ_e for pre-*Matthew* on 20–22 and 24 September. The bold curves mark the first and last days of the sequence, and the number on each curve shows the date. This figure is available in colour online at wileyonlinelibrary.com/journal/qj

vorticity would lead to the spin-up of the system. This effect is argued to be an explanation for why tropical-wave-scale mid-level vortices foster tropical storm formation.

While we have several concerns about Raymond and Sessions' formulation of the problem[‡], it is nonetheless pertinent to enquire whether there is observational support in the PREDICT data for the configuration envisaged by Raymond and Sessions. As noted above, from the data shown in Figures 13 and 15, we do not find cooling[§] of air below 10 km in altitude on the scale of the pouch. Rather, in all developing cases there is slight warming.

While the analyses of CAPE shown here are not useful for distinguishing between developing and non-developing systems, they do indicate significant levels of CAPE in the pouch region of the disturbances analysed. Approximately 50% of soundings had CAPE values exceeding 1500 J kg^{-1} and approximately 10% had values exceeding 2500 J kg^{-1}. This finding is in sharp contrast to the idea conveyed in Emanuel *et al.* (1994) that levels of CAPE over the tropical oceans are minimal, sufficient only to offset the dissipation within clouds. However, we acknowledge that the way in which we define CAPE is different from that of Emanuel *et al.*, who use a definition that assumes reversible adiabatic displacements. Their definition includes the effects of condensed water on air parcel buoyancy and applies to non-precipitating convection. On the basis of our observations, we would argue that the levels of CAPE in the pouch region of tropical disturbances are not insignificant and are adequate to support modes of convective organization just as in the middle latitudes over land.

6. Conclusions

This work was carried out to determine the salient thermodynamic characteristics of the 'pouch region' of developing and non-developing tropical disturbances. To this end, we have presented an analysis of the dropwindsonde data obtained for the most extensively documented pre-depression disturbances during the PREDICT, GRIP and IFEX experiments, which were conducted during the peak of the 2010 Atlantic hurricane season. In particular, we describe three cases which were extremely well sampled both spatially and temporally. The analyses provide unprecedented quantitative information about the vertical structure, magnitude, and range of variability of important thermodynamic quantities such as virtual potential temperature, relative humidity and equivalent potential temperature.

We calculated the mean sounding of virtual potential temperature and pseudo-equivalent potential temperature on each day for the pouch region of the disturbances. The departures from the system mean averaged over the four or five (mostly consecutive) days of observations was presented also. For the two developing disturbances (*Karl* and *Matthew*) in the Caribbean region and for the system that failed to redevelop (ex-*Gaston*), there was a slight to moderate warming in virtual potential temperature through much of the troposphere during the four or five days of observations, but no obvious change in dry static stability.

Two notable paradigms that have been offered previously to explain tropical cyclogenesis have assumed a modest cooling of the lower troposphere. This presumption is not supported by the PREDICT–GRIP observations on the scale of the pouch.

In contrast to the developing cases, the equivalent potential temperature in the non-developing ex-*Gaston* showed a higher degree of variability, which was found to be largely associated with that in the water vapour mixing ratio.

All systems had significant amounts of CAPE, with 50% of soundings having values in excess of 1500 J kg^{-1} and 10% in excess of 2500 J kg^{-1}. Soundings with high values of CAPE tended to have low values of CIN. Interestingly,

[‡]First, the temperature and moisture perturbations imposed in the model are based on observational data taken within a mesoscale convective vortex embryo and proximity soundings of the same mesoscale convective system. It would be fortuitous if these proximity soundings were representative of the radiative-convective equilibrium state of the entire tropical disturbance. Indeed, the vortex embryo is highly unlikely to be in a radiative-convective equilibrium state (Brown and Bretherton, 1997). Nevertheless, the foregoing perturbations are treated as perturbations to the radiative-convective equilibrium state of the tropical disturbance. Second, the research flights in TEXMEX were typically at 700 mb and thus the data obtained were unable to document the convective environment through the troposphere. Third, without ambient rotation and without a truly three-dimensional configuration of the model, these experiments cannot offer insight into the dynamics of the segregation and aggregation of vorticity as discussed above. It is yet to be demonstrated whether the thermodynamic control as envisaged by Raymond and Sessions is essential in a rotational environment.

[§]Although we present fields of virtual potential temperature, the temperature fields exhibit the same day-to-day evolution (not shown).

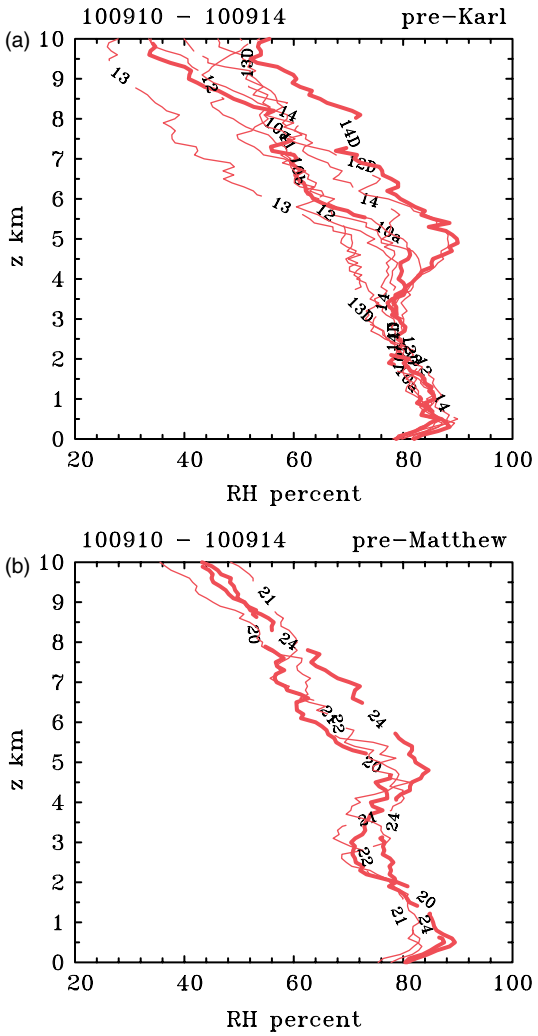

Figure 16. Vertical profiles of departures from mean profiles of system-mean relative humidity on all days for (a) pre-*Karl* during the period 10–14 September, and (b) pre-*Matthew* during the period 20–24 September. The bold curves mark the first and last days of the sequence. The number on each curve shows the date; the letter 'D' denotes a DC-8 flight. This figure is available in colour online at wileyonlinelibrary.com/journal/qj

the largest values (> 3000 J kg^{-1}) were found in ex-*Gaston*. These findings are in sharp contrast to the idea conveyed in Emanuel *et al.* (1994) that levels of CAPE over the tropical oceans are minimal, sufficient only to offset the dissipation within clouds. Indeed, it would appear that levels of CAPE in the pouch region of tropical disturbances are not insignificant and are adequate to support modes of convective organization. Even so, the evolution and distribution of CAPE and CIN by themselves did not reveal an obvious distinction between developing and non-developing systems. Perhaps the most potentially significant difference between the developing and non-developing systems was the smaller difference in pseudo-equivalent potential temperature at the surface and the mid-tropospheric minimum of this quantity. This difference was about 15–17 K in the developing systems compared with about 25 K in the non-developing system, ex-*Gaston*.

These observations provide a context for future study of the interaction between the pouch and its environment and of the development of rotating deep convection within the pouch. Both of these topics are important elements of the marsupial paradigm and research efforts in both directions are currently underway.

Acknowledgements

We are grateful to Mark Boothe for providing the consensus pouch tracks, assistance with some of the code checking and for his assistance with finalizing the two figures depicting the GV flight tracks, dropsondes and infrared satellite imagery for the pre-*Karl* disturbance. We thank also Ed. Zipser and an anonymous reviewer for their perceptive comments on the original manuscript; and Gerald Thomsen and Gerard Kilroy for their comments on a near-final version of the revised version. We acknowledge the US National Science Foundation for their support of the PREDICT experiment. MTM acknowledges the support of NSF AGS-0733380 and NSF AGS-0851077, NOAA's Hurricane Research Division and NASA grants NNH09AK561, NNG11PK021 and NNG09HG031. RKS acknowledges financial support for tropical-cyclone research from the German Research Council (Deutsche Forschungsgemeinschaft) from grant number SM30/25-1.

Appendix

Calculation of CAPE and CIN

The values of CAPE and CIN given in this article are calculated by lifting hypothetical air parcels from the surface and from heights of 100–500 m above the surface at 100 m intervals until the LNB of the particular parcel. Pseudo-adiabatic ascent is assumed and the latent heat of fusion in the upper troposphere is not accounted for. Integrals of the buoyancy force, proportional to the difference between the virtual temperature of a lifted parcel and that of its environment at a given height, are evaluated over the height ranges of positive buoyancy and negative buoyancy using a trapezoidal method with a height interval of 100 m. The sum of the positive and negative integrals for the parcels lifted from 100–500 m is then averaged to give the CAPE. The value of the integral for the parcel lifted from the surface is omitted as, in some cases, it can be as much as twice the value at 100 m, calling into question its representativeness. We define the CIN as the minimum value of the six negative integrals (including the surface lifted parcel). The reader is reminded that these methods for calculating CAPE and CIN, like any others, are arbitrary and other methods will give different values. For example, if CAPE is defined solely on the basis of the value for an air parcel lifted from the surface, much larger values may arise.

The calculations use Bolton's formula (Bolton, 1980) to evaluate the pseudo-equivalent potential temperature and the formula given in Emanuel (1994, p 116, Eq. 4.4.13) is used to calculate the saturation vapour pressure.

References

Bister M, Emanuel KA. 1997. The genesis of hurricane *Guillermo*: TEXMEX analyses and a modeling study. *Mon. Weather Rev.* **125**: 2662–2682.

Bolton D. 1980. The computation of equivalent potential temperature. *Mon. Weather Rev.* **108**: 1046–1053.

Braun SA, Montgomery MT, Mallen KJ, Reasor PD. 2010. Simulation and interpretation of the genesis of tropical storm *Gert* (2005) as part of the NASA Tropical Cloud Systems and Processes Experiment. *J. Atmos. Sci.* **67**: 999–1025.

Brown RG, Bretherton CS. 1997. A test of the strict quasi-equilibrium theory on long time and space scales. *J. Atmos. Sci.* **54**: 624–638.

Cotton WR, Anthes RA. 1989. *Storm and cloud dynamics*. Academic Press: San Diego, CA. pp 883.

Davis CA, Ahijevych DA. 2012. Mesoscale structural evolution of three tropical weather systems observed during PREDICT. *J. Atmos. Sci.* **69**: in press.

Dunkerton TJ, Montgomery MT, Wang Z. 2009. Tropical cyclogenesis in a tropical wave critical layer: easterly waves. *Atmos. Chem. Phys.* **9**: 5587–5646.

Elsberry RL, Harr P. 2008. Tropical cyclone structure (TCS08) Field experiment scientific basis, observational platforms, and strategy. *Asia-Pacific J. Atmos. Sci.* **44**: 1–23.

Emanuel KA. 1989. The finite amplitude nature of tropical cyclogenesis. *J. Atmos. Sci.* **46**: 3431–3456.

Emanuel KA. 1994. *Atmospheric convection.* Oxford University Press, Oxford, UK.

Emanuel KA, Neelin JD, Bretherton CS. 1994. On large-scale circulations in convecting atmospheres. *Q. J. R. Meteorol. Soc.* **120**: 1111–1143.

Fang J, Zhang F. 2010. Initial development and genesis of hurricane *Dolly* (2008). *J. Atmos. Sci.* **67**: 655–672.

Fierro AO, Zipser EJ, Lemone MA, Straka JM, Simpson J. 2012. Tropical oceanic hot towers: need they be dilute to transport energy from the boundary layer to the upper troposphere effectively? An answer based on trajectory analysis of a simulation of a TOGA COARE convective system. *J. Atmos. Sci.* **69**: 195–213.

Frank WM. 1987. Tropical cyclone formation. In: *A global view of tropical cyclones*. Elsberry RL (ed.) Office of Naval Research, 53–90.

Halverson J, Black M, Rogers R, Braun S, Heymsfield G, Cecil D, Goodman M, Hood R, Heymsfield A, Krishnamurti TN, McFarquhar G, Mahoney MJ, Molinari J, Turk J, Velden C, Zhang D-L, Zipser EJ, Kakar R. 2007. NASA's Tropical Cloud Systems and Processes Experiment. *Bull. Amer. Meteorol. Soc.* **88**: 867–882.

Haynes P, McIntyre ME. 1987. On the evolution of vorticity and potential vorticity in the presence of diabatic heating and frictional or other forces. *J. Atmos. Sci.* **44**: 828–841.

Hendricks EA, Montgomery MT, Davis CA. 2004. On the role of 'vortical' hot towers in formation of tropical cyclone *Diana* (1984). *J. Atmos. Sci.* **61**: 1209–1232.

Hiroshi A. 1978. A method of bivariate interpolation and smooth surface fitting for irregularly distributed data points. *ACM Trans. Math. Software* **4**: 148–164.

Hiroshi A. 1984. On estimating partial derivatives for bivariate interpolation of scattered data. *Rocky Mountain J. Math.* **14**: 41–52.

Holton JR. 2004. *An introduction to dynamic meteorology*. Academic Press: London.

Houze RA. 1993. *Cloud dynamics*. Academic Press: San Diego, CA. pp 573.

Houze RA, Lee W-C, Bell MM. 2009. Convective contribution to the genesis of hurricane *Ophelia* (2005). *Mon. Weather Rev.* **137**: 2778–2800.

James RP, Markowski PM. 2009. A numerical investigation of the effects of dry air aloft on deep convection. *Mon. Weather Rev.* **137**: 140–161.

Karyampudi VM, Pierce HF. 2002. Synoptic-scale influence of the Saharan air layer on tropical cyclogenesis over the eastern Atlantic. *Mon. Weather Rev.* **130**: 3100–3128.

McBride JL. 1995. Tropical cyclone formation. 21–62 in *Global Perspectives on Tropical Cyclones*. Elsberry RL (ed.) WMO/TD-No 693, World Meteorological Organization: Geneva, Switzerland.

Montgomery MT, Smith RK. 2011. Tropical cyclone formation: Theory and idealized modelling. In *Proceedings of Seventh WMO International Workshop on Tropical Cyclones (IWTC-VII)*, La Réunion, Nov. 2010. (WWRP 2011-1) World Meteorological Organization: Geneva, Switzerland.

Montgomery MT, Nicholls ME, Cram TA, Saunders AB. 2006. A vortical hot tower route to tropical cyclogenesis. *J. Atmos. Sci.* **63**: 355–386.

Montgomery MT, Nguyen SV, Smith RK. 2009. Do tropical cyclones intensify by WISHE? *Q. J. R. Meteorol. Soc.* **135**: 1697–1714.

Montgomery MT, Davis C, Dunkerton T, Wang Z, Velden C, Torn R, Majumdar S, Zhang F, Smith RK, Bosart L, Bell MM, Haase JS, Heymsfield A, Jensen J, Campos T, Boothe MA. 2012. The Pre-Depression Investigation of Cloud systems in the Tropics (PREDICT) experiment: Scientific basis, new analysis tools, and some first results. *Bull. Amer. Meteorol. Soc.* **93**: 153–172.

Nguyen SV, Smith RK, Montgomery MT. 2008. Tropical-cyclone intensification and predictability in three dimensions. *Q. J. R. Meteorol. Soc.* **134**: 563–582.

Ooyama KV. 1969. Numerical simulation of the life cycle of tropical cyclones. *J. Atmos. Sci.* **26**: 3–40.

Raymond DJ, Sessions SL. 2007. Evolution of convection during tropical cyclogenesis. *Geophys. Res. Lett.* **34**: L06811, DOI: 10.1029/2006GL028607.

Reasor PD, Montgomery MT, Bosart LF. 2005. Mesoscale observations of the genesis of hurricane *Dolly* (1996). *J. Atmos. Sci.* **62**: 3151–3171.

Ritchie EA, Holland GJ. 1999. Large-scale patterns associated with tropical cyclogenesis in the western Pacific. *Mon. Weather Rev.* **127**: 2027–2043.

Rutherford B, Montgomery MT. 2011. A Lagrangian characterization of a developing and non-developing disturbance observed during the PREDICT Experiment. *Atmos. Chem. Phys. Discuss.* **11**: 33272–33323.

Saunders AB, Montgomery MT. 2004. 'A closer look at vortical hot towers within a tropical cyclogenesis environment'. Atmospheric Science Bluebook No. 752. Colorado State University: Fort Collins, USA.

Shay LK. 2010. Air–sea interactions. Chapter 42 of *Global perspectives on tropical cyclones: From science to mitigation.* Kepert JD, Chan JCL (eds). *Series on Asia-Pacific Weather and Climate*, vol. 4. World Scientific: Singapore.

Stith JL, Haggerty JA, Heymsfield A, Grainger CA. 2004. Microphysical characteristics of tropical updrafts in clean conditions. *J. Appl. Meteorol.* **43**: 779–794.

Stommel H. 1947. Entrainment of air into a cumulus cloud. *J. Meteorol.* **4**: 91–94.

Tory KJ, Montgomery MT. 2007. Internal influences on tropical cyclone formation. In *Proceedings of Sixth WMO International Workshop on Tropical Cyclones (IWTC-VI)*, San José, Costa Rica, Nov. 2006. (WWRP 2007-1) World Meteorological Organization: Geneva, Switzerland.

Tory K, Frank WM. 2010. Tropical cyclone formation. Chapter 2 of *Global perspectives on tropical cyclones: From science to mitigation*. Kepert JD, Chan JCL (eds). *Series on Asia-Pacific Weather and Climate*, vol. 4. World Scientific: Singapore.

Wissmeier U, Smith RK. 2011. Tropical-cyclone convection: the effects of ambient vertical vorticity. *Q. J. R. Meteorol. Soc.* **137**: 845–857.

Zipser EJ, Twohy CH, Tsay S-C, Hsu NC, Heymsfield GM, Thornhill KL, Tanelli S, Ross R, Krishnamurti TN, Ji Q, Jenkins G, Ismail S, Ferrare R, Chen G, Browell EV, Anderson B, Hood R, Goodman HM, Heymsfield A, Halverson J, Dunion JP, Douglas M, Cifelli R. 2009. The Saharan Air Layer and the fate of African Easterly Waves – NASA's AMMA field study of tropical cyclogenesis. *Bull. Amer. Meteorol. Soc.* **90**: 1137–1156.

